Building and Environment 248 (2024) 111096

Contents lists available at ScienceDirect

Building and Environment

journal homepage: www.elsevier.com/locate/buildenv

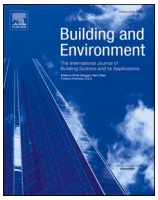

Influence of cross-ventilation cooling potential on thermal comfort in high-rise buildings in a hot and humid climate

Roberto Stasi [a,*], Francesco Ruggiero [a], Umberto Berardi [b]

[a] Department of Architecture, Built Environment and Design, Polytechnic University of Bari, Via Edoardo Orabona, 4, 70126, Bari, Italy
[b] Department of Architectural Science, Toronto Metropolitan University, 350 Victoria St, Toronto, Canada

ARTICLE INFO

Keywords:
CFD
Cross-ventilation
Adaptive comfort model
Passive cooling
Natural ventilation
Building form

ABSTRACT

The rising cooling energy demand, caused by the increase in global average temperature and the frequency of heat waves, is currently leading to a significant increase in global electricity consumption. Passive cooling strategies, such as ventilative cooling, can provide acceptable indoor thermal comfort with no or minimal energy consumption, offering an alternative to air conditioning systems in buildings. This paper investigates the effectiveness of natural ventilation in an iconic post-modernist high-rise building in India: Charles Correa's Kanchanjunga Apartments. The research, employing CFD simulation paired with building energy simulation, demonstrates how cross-ventilation can improve the ventilative cooling efficiency in buildings, ensuring affordable indoor thermal conditions even in adverse climatic conditions like the Indian one. Thanks to night-time structural cooling, a maximum reduction in the operative temperature of up to 5.3 °C was achieved compared to the scenario without natural ventilation and up to 6.4 °C compared to the outdoor temperature peak on the hottest day. Consistently with the Indian Model for Adaptive Comfort, cross-ventilation ensures a reduction in discomfort hours of up to 58 % on the hottest day and a total reduction in discomfort hours on a typical monsoon and winter day. The paper aims to assist architects and policymakers in quantifying the cooling potential of natural ventilation in high-rise buildings, suggesting passive solutions for cooling energy saving.

1. Introduction

The steady increase in global average temperature as a direct result of global warming [1], as well as the raising frequency and intensity of extreme events like heatwaves [2], are causing ambient temperatures to rise, leading to overheating problems in buildings [3,4].

This phenomenon, powered by the worldwide spread of the International Style [5], the change of comfort expectations [6], the increase of indoor thermal gains, the exacerbation of the urban heat island impact [7,8], as well as the side effects of progressing optimization in the building envelope to reduce heating consumptions, are leading to a significant increase in global cooling energy demand, driven by the increased use of air conditioning in buildings [9]. The marked rise in electricity consumption for cooling and the resulting peak power demand, which currently depends on fossil fuels, worsens the environmental impact of buildings and reduces the effectiveness of energy-saving and greenhouse gas emission reduction policies [10].

Between 1950 and 1980, there was a 33 % rise in population-weighted annual cooling days, which persisted between 1981 and 2017, with an average yearly increase of 0.9 cooling degree days (CDD) [11]. As underlined by the latest IPCC report [12], this trend is predicted to exacerbate in the coming years, with the most substantial increase expected to impact the entirety of southern Europe [13], China [14,15], India [16], and the United States [17].

Research on cooling demand under future climate change scenarios shows that cooling electricity consumption could double in most European countries [18] and reach an increase of 15–126 % even in heating-dominated climates like Canada [19]. However, the most significant growth is expected in the energy needs of emerging economies. Notably, in China, the increase in electricity consumption for cooling is projected to rise by up to 7.5 times under the RCP 4.5 scenario [20]. Likewise, in Brazil, energy consumption is forecast to increase between 70 % and 190 % by 2100 [21]. India will experience a 45 % increase by 2030 [22], and the potential cooling demand for the city of Mumbai in India alone is estimated to be almost 24 % of the total cooling demand of the United States [23]. According to Khourchid et al. [24], by the middle of the 21st century, the average increase in building cooling electricity demand could reach 33 %, 89 %, 288 % and 376 % in tropical, arid, cold and temperate climates, respectively. Increased electricity consumption

* Corresponding author.
E-mail addresses: roberto.stasi@poliba.it (R. Stasi), francesco.ruggiero@poliba.it (F. Ruggiero), uberardi@torontomu.ca (U. Berardi).

https://doi.org/10.1016/j.buildenv.2023.111096
Received 23 August 2023; Received in revised form 11 November 2023; Accepted 1 December 2023
Available online 5 December 2023
0360-1323/© 2023 The Authors. Published by Elsevier Ltd. This is an open access article under the CC BY license (http://creativecommons.org/licenses/by/4.0/).

Nomenclature

ALD	ASHRAE Likelihoodod of Dissatisfied
ACH	Air Change Rate
BES	Building Energy Simulation
CDD	Cooling degree days
CFD	Computational fluid dynamics
CV	Cross-ventilation
IAQ	Indoor Air Quality
IEA	International Energy Agency
IMAC	Indian Model for Adaptive Comfort
IPCC	Intergovernmental Panel on Climate Change
LPD	Long-term Percentage of Dissatisfied
NV	Natural ventilation
PMV	Predicted Mean Vote
POR	Percentage Outside the Range
PPD	Predicted Percentage of Dissatisfied
RANS	Reynolds-Averaged Navier-Stokes
SHGC	Solar Heat Gain Coefficient
SST	Shear Stress Transport
SSV	Single-sided ventilation
TMY	Typical Meteorological Year
WD	Wind Driven ventilation
WWR	Windows-to-Wall Ratio

Symbology

h_i	occupancy hours
k	von Karman constant
t_a	average air temperature
t_o	operative temperature
t_r	mean radiant temperature
u^*	friction velocity
u_{ref}	reference wind speed
z_{ref}	reference height
v_r	relative air velocity
ε	turbulence dissipation rate
ω	specific dissipation rate

to provide cooling thermal comfort in buildings will reduce the reliability of the electricity grid, leading to more frequent power outages and additional pressure on the grid [25–27].

Additionally, by the year 2050, more than 68 % of the world's population is expected to live in urban areas, with a pronounced concentration foreseen in the Global South [28]. A significant percentage of these areas will be in developing countries, mainly in tropical regions, where access to cooling services in buildings remains severely limited.

While Global North is currently turning to air conditioning to mitigate the effects of global warming, this option is not available to everyone [29]. Rising ambient temperatures, coupled with potentially inadequate building design and a lack of resources for the use of mechanical cooling systems, have forced a significant percentage of the world's population, more than one billion people worldwide, to live in very uncomfortable indoor temperatures [30].

As climate change makes space cooling a necessity for survival, ensuring that cooling needs are met equitably becomes paramount. In fact, by helping to maintain thermal comfort in buildings, space cooling systems are proving to be the primary defense against mortality risk for the most vulnerable members of the population by counteracting the potential health effects of excessive heat [31–33]. In Global South countries such as India, where economic constraints primarily limit the use of air conditioning, mortality rates have been observed to increase by more than 18.1 % during heat-wave episodes compared to non-heat-wave periods, peaking at 29.9 % in Jaipur [34].

Consequently, the economic or physical total lack of energy access stresses the importance of exploring alternative passive approaches to air conditioning to cope with the health risks associated with the inevitable trajectory of climate change and ensure improved indoor comfort within the buildings [35,36].

1.1. Passive ventilative cooling and building resilience

To effectively integrate energy-efficient building design to deal with the forthcoming increase in cooling-related energy demands, passive cooling strategies, such as natural ventilation (NV) in buildings, can ensure acceptable indoor comfort levels by reducing the mechanical cooling energy consumption and increasing buildings resilience to climate change and stress [37,38].

According to IEA Annex 80 [39], the idea of thermal resilience in buildings is closely linked to the principles of passive architecture, which emphasizes the ability of a building to protect its occupants from external climatic events while providing indoor comfort conditions, primarily through natural means. Mainly focusing on the cooling season and the overheating risk, building design and, even more, passive cooling strategies can highly influence thermal indoor comfort [40,41]. So, on the way to slowing the growth of electricity consumption, reducing the cost of peak electricity, avoiding the risk of blackouts and further CO_2 emissions in the building sector, it's clear that alternatives to the increased use of energy-intensive air conditioning are needed.

As indicated by the IEA Annex 62 [42], ventilative cooling (VC) exploits the cooling potential of the outside airflow through the use of natural solutions, either wind-driven or buoyancy-driven, or mechanical technologies or a combination of both (i.e. mixed or hybrid ventilation) to reduce or even eliminate the cooling loads and the energy use by mechanical cooling in buildings, while ensuring a comfortable thermal environment. From this perspective, the cooling potential offered by natural ventilation is still proving to be an effective and promising solution [43–45] for cooling energy saving in buildings [46,47] while ensuring indoor air quality (IAQ) and acceptable levels of thermal comfort [48,49].

There are various ways natural ventilation can exploit its ventilative cooling potential depending on the global and local climatic site conditions [50,51]. These include *structural cooling* based on increasing ventilation air flows, especially at night, to cool the thermal mass of buildings and reduce cooling loads during the day [52,53], *free cooling* achieved by cooling the indoor air temperature with lower temperature outdoor air exchange [54,55] and *comfort cooling* obtained by direct air flows over the human body that can reduce heat perception by increasing convective exchange due to both the temperature difference between air and skin and air velocity [56–58].

Several studies have discussed how natural ventilation can improve thermal comfort [59,60] and energy performance of buildings [61–63] even in a future driven by climatic changes [64–66]. Undoubtedly, the effectiveness of natural ventilation systems, depending on the variability of external climatic conditions, turns operating mode essential to manage and benefit from them [67,68]. In addition, the main research findings on the cooling potential of natural ventilation highlighted its strong dependence on building morphology. In fact, the effectiveness of natural ventilation in providing indoor air quality and passive cooling in buildings is strictly dependent on the design of the building itself [69,70].

Ventilation systems that rely solely on natural forces, such as wind and thermal buoyancy, must be designed with the building in mind, as the building itself and its spatial elements are the main factors that can reduce or increase the air movement and influence its content [82]. For

these systems to be effective, it is necessary to optimize the generation and employment of natural air paths inside the building by increasing their speed and improving the distribution of indoor ventilation working on its reliance on building shape [71]. Contrary to the current trend, where air-conditioning has made architectural styles international rather than regional and lost their relationship with the environment and natural forces, increasing the efficiency of natural ventilation by optimizing building form will be crucial to reducing the carbon footprint of today's buildings.

1.2. CFD for natural ventilation

Among several natural ventilation strategies, wind-driven cross-ventilation (CV) is undoubtedly recognized as the most effective ventilation method for buildings, especially if cooling loads are to be reduced [72].

Compared to single-side ventilation (SSV), CV ensures higher ventilation rates and more effective ventilative cooling capacity, providing better indoor comfort conditions [73]. As pointed out by Omrani et al. [74], CV can maintain comfortable conditions for 70 % of the time, compared to just 1 % for single-sided ventilation, ensuring an air change rate 14 times higher than SSV one [75].

To improve the cross-ventilation potential, air must flow freely within the building. The most critical factor for achieving optimal cross-ventilation efficiency is ensuring the continuity of internal spaces. This will enable effective communication between the windward and leeward sides, thus maximizing the internal airflow, which is dependent on the pressure difference induced by the wind on the building façades [76]. Indeed, the spatial layout, determining how different areas are connected to one another, is a crucial factor in the performance of natural ventilation systems [77].

Due to the complexity of assessing the wind-driven cross-ventilation potential in buildings, computational fluid dynamics (CFD), alongside experimental research, both field measurements [78–81] and wind tunnel experiments [82–84], have been employed widely. Indeed, CFD allows researchers to investigate complex ventilation issues that may be difficult or infeasible to analyze using alternative approaches [85].

Several researchers have used CFD analysis to investigate how the morphological characteristics of buildings can affect air distribution in confined spaces depending on wind direction and intensity [86,87], urban surroundings [88–90], building geometry [59,91–94], façade geometrical details [95–97] and position and size of the ventilation openings [98–100].

Large Eddy Simulations (LES) [50,89] and Reynolds-Averaged Navier-Stokes (RANS) simulations [59,92,101] have been involved as the most common CFD models for assessing indoor airflow associated with cross-ventilation. Actually, LES performs more accurate results [102,103]; however, due to more intensive computational resources needed, most of the studies in the literature adopt the RANS equation as a turbulence closure model. The selection of turbulence models relies on the particular problem to be resolved. It is crucial to pay special attention to this aspect as it significantly affects the precision of simulation outcomes [104].

Faced with this problem, Péren et al. [105] assessed the suitability of various turbulence models, including the standard k-epsilon, RNG and Shear-Stress-Transport (k-ω SST), for isothermal analysis of natural ventilation in a cross-ventilated building. Consequently, they found that the k-ω SST model exhibited the most robust agreement with experimental data. The same conclusion was also reached by further studies of Ramponi et al. [106], Wang et al. [48] and Mohotti et al. [107].

Actually, the majority of research has focused on single zones or indoor environments lacking internal partitions. Although this approach provides valuable theoretical insights, it ignores the actual spatial layout of real buildings and neglects the relationships in the airflow path between multiple zones.

Even when analyzing entire buildings, it often only relies on idealized or archetypal models, focusing primarily on airflow within the building as a stand-alone analysis, rather than considering the impact of airflow on thermal comfort conditions or acceptable levels of air change and velocity.

Moreover, if a comprehensive examination of the entire building has been conducted, it is typically completed solely through a CFD analysis of the indoor environment by employing air velocity as an inlet boundary condition. Although this simplifies the analysis, it does not consider possible airflow deviations due to wind-induced pressure field distributions on the building.

When assessing the thermal comfort of occupants in cross-ventilated buildings, it is important to prioritize the distribution of air velocities and average air velocity in indoor spaces over the ventilation flow rate. Hence, the capability to predict the influence of the building's form on the thermal comfort of indoor spaces and the airflow interaction between multiple zones holds a considerable impact on the building design.

Employing comprehensive building simulations to investigate airflow patterns and assessing the connection between this analysis and its impact on a building's thermal performance and occupants' comfort perception represents a novel and evolving methodology. This approach involves integrating building energy simulations (BES) with computational fluid dynamics tools, thereby creating a precise and efficient means to enhance the evaluation of energy requirements and thermal comfort within buildings [108–110].

Along this line, the present study tries to provide more accurate results on the effect of cross ventilation on thermal comfort in buildings by combining CFD analysis with BES. Contrary to existing studies, where the BES analysis is used to define the boundary conditions of the CFD analysis, the novelty of the study lies in the implementation of the airflow properties measured by CFD analysis into the BES to dynamically evaluate cross-ventilation's influence on thermal comfort.

The main objective is to propose a novel comprehensive methodological approach through airflow simulations in multiple digital environments to investigate the cooling potential of natural ventilation in real high-rise buildings from the outdoor environment to the indoor thermal comfort evaluation.

In contrast to the models commonly used in CFD comfort analysis, relayed on the Fanger model or the ASHRAE adaptive model, which neglect the true adaptability of humans in hot climates, the applicability of a recent alternative model of adaptive comfort, called IMAC (Indian Model for adaptive comfort), is evaluated to improve the thermal comfort acceptability limits and the sustainability of the built environment in hot and humid climates.

Undoubtedly, the struggling challenge in empowering cross-ventilation potential within the buildings is to ensure spatial continuity between the windward and leeward sides against the indoor spaces' layout needs. This objective turns out to be even more complex when dealing with high-rise buildings, where, due to the high-density building typology, the main design effort is made to maximize the number of apartments available on the same floor.

Due to the increasing growth of high-rise buildings and their importance in modern architecture, this study highlights the role of cross-ventilation on indoor thermal comfort and proposes guidelines for more efficient indoor ventilation performance for this building typology. Therefore, the potential of ventilative cooling in an emblematic naturally ventilated post-modernist architecture high-rise building is evaluated to provide benchmarks for current buildings design.

2. Case study

2.1. Building characteristics

This paper investigates the fluid dynamic and thermal behaviour of a naturally ventilated high-rise building in India, the Kanchanjunga Apartments, designed by the Indian architect Charles Correa (Fig. 1).

Fig. 1. Kanchanjunga Apartments external view: a) South-Est Façade, b) South-Est terrace view, c) South-West Façade, d) North-West terrace, e) double-height living room.

The building is one of Correa's most famous projects and one of the milestones of post-modern architecture. Built in 1983 in Mumbai in north-eastern India, the 85-m tower is named after the second-highest mountain in the Himalayas.

Kanchanjunga Apartments is a 28-storey apartment building with 32 duplex apartments, two on each floor. In this building, the architect elaborates a brand-new design way to devise a high-rise building through a complex study of the building section (Fig. 2). Mumbai's climate and location present the architects with a contradictory situation: the East-West axis is the best orientation to take advantage of wind action and capture sea breezes, but it exposes the building's surfaces to the high afternoon sun and monsoon rains.

In addressing this issue, the architect decided to open up the building in the direction of the prevailing winds by placing large air-permeable openings only on these sides. In a spatial arrangement reminiscent of a traditional Indian bungalow, the architect enveloped the central living spaces with verandas and double-height terraces. These buffer zones effectively shield the living areas from the sun's rays and allow the opening surfaces to be modulated to improve natural cross-ventilation in the interior without exposing them to direct solar radiation.

The square building (21 × 21 m) is formed by intertwining four distinct apartment units featuring slight level variations on the floor. This arrangement creates a mesh of two 4-bedroom and two 6-bedroom units ranging from 180 to 420 square meters. Specifically, Type A comprises ten units, accommodating up to six residents plus a servant's room. In this unit, verandas to the north-west and a double-height terrace to the south-east are placed. The main part of the dwelling unit is on two floors, connected by a mezzanine floor facing the prevailing winds. Type B is the smallest accommodation. It has three rooms for a total of five people. It has verandas on the south-east façade and a

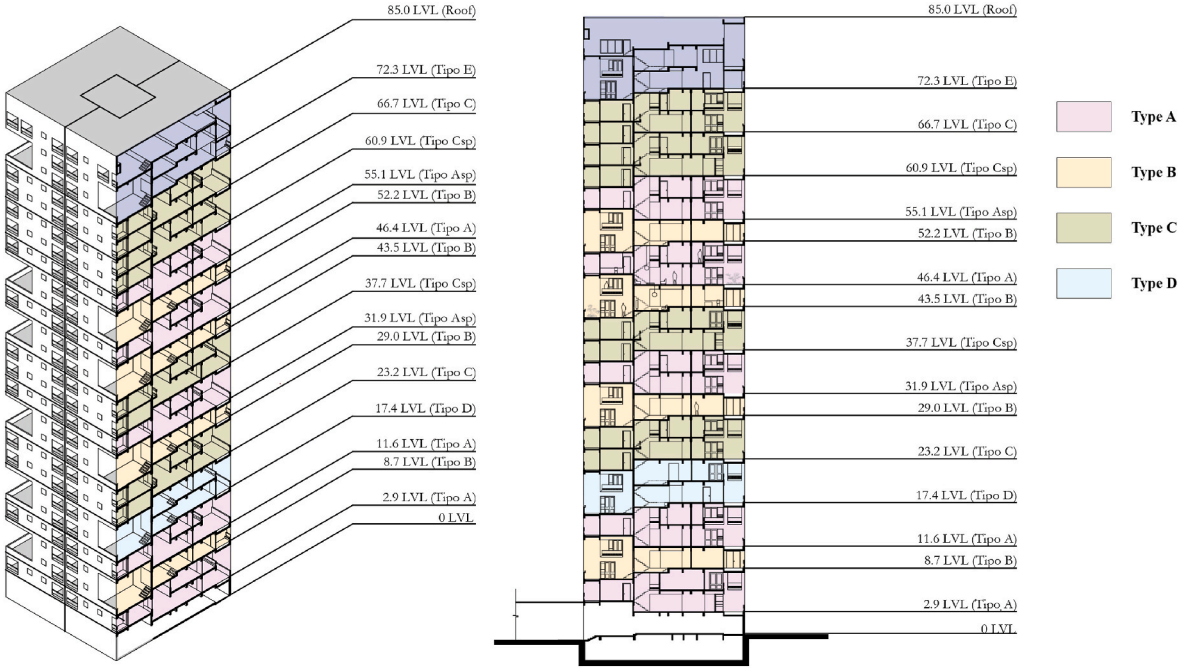

Fig. 2. Axonometric cross-section and 2D cross-section of Kanchanjunga Apartments.

double-height terrace on the north-west façade.

Type C has two main floors connected by two staggered mezzanines. It is suitable for ten people and is characterised by a double veranda profile on the north-west windward side and a double-height terrace on the south-east side. Finally, type D, present in only two units, is characterised by a double-height terrace on both sides and is the only type that does not have double-height spaces within it. All units are characterised by connecting elements and double-height spaces in the centre, which become central elements to connect the windward and leeward sides of the building, allowing free airflow through cross-ventilation. The slight changes in height between the different functional spaces of the house, as well as the creation of a hierarchy between the spaces, minimise the presence of physical obstacles to airflow pathway.

Among the several typology units of the building, the analysis was carried out on the one identified as Type A, which represents the most recurring unit in the building. In particular, the one located at 35 m above ground level to avoid the influence of the surroundings on the wind flow and facing west was studied, as it represents the worst situation for cooling demand due to solar load. Fig. 3 shows the main architectural features of the selected typology. The apartment has a total volume of 675 m^3 and a total floor surface of 196.70 m^2 on three levels. The windows-to-wall ratio (WWR) is equal to 17.40. The total window opening area is 31.9 m^2, with 7 m^2 on the windward side and 24.9 m^2 on the leeward one. The inlet-to-outlet ratio (A_{in}/A_{out}) results equal to 0.28.

2.2. Site and climate

Mumbai belongs to climate zone Aw (tropical savannah climate) according to the Köppen-Geiger classification.

Typical climatic conditions include mild, dry winters and humid, hot summers. The average annual temperature is 26.7 °C. During the hottest month, April, the outdoor temperature reaches 38.5 °C, while during the coldest months, it remains above 18 °C, rarely falling below 15 °C. The daily and annual temperature ranges are high, especially in winter. The building is oriented 295° N, therefore, with the main façades facing northwest and southeast.

Regarding wind site characteristics, Mumbai, influenced by its proximity to the sea, experiences high wind velocity throughout the year. The prevailing winds are concentrated between the N and W directions. The average annual wind speed is 5.5 m per second, and the average maximum wind speed is more than 10.5 m per second. The main climatic characteristics of the city of Mumbai are summarized in Table 1.

3. Methodology

In the present work, a novel comprehensive modelling approach across multiple digital environments was carried out to assess the ventilative cooling potential of cross-ventilation on thermal comfort in the case study. The analysis consisted in four steps, as shown in Fig. 4.

Firstly, a 3D RANS equations with k–ω SST turbulence model simulation was performed in the external environment to evaluate the wind-induced pressures on the building surfaces using Ansys Fluent.

By measuring the average pressures at the building openings, the behaviour of wind-driven natural indoor ventilation was simulated to evaluate the indoor air distribution and the average air velocity inside the building due to cross-ventilation, using the building envelope of a Type A apartment as the CFD domain. The previous step's indoor airflow characteristics were utilized to assess the impact of natural ventilation on the building's thermal performance via a thermal dynamic analysis carried out on DesignBuilder (DB) on an hourly basis, across three

Table 1
Mumbai climatic site characteristics.

Location	Mumbai
Latitude	18° 57′ 53″ N
Longitude	72° 49′ 33″ E
Prevalent wind	NNW
Average wind speed	5.5 m/s
Köppen-Geiger climate classification	Aw
Average yearly temperature	26.7 °C
Outdoor T_{max}	38.5 °C (5th April)
Outdoor T_{min}	14.2 °C (2nd January)
Max direct solar radiation	*2019*.56 kWh/m^2

Fig. 3. Architectural project apartment type A.

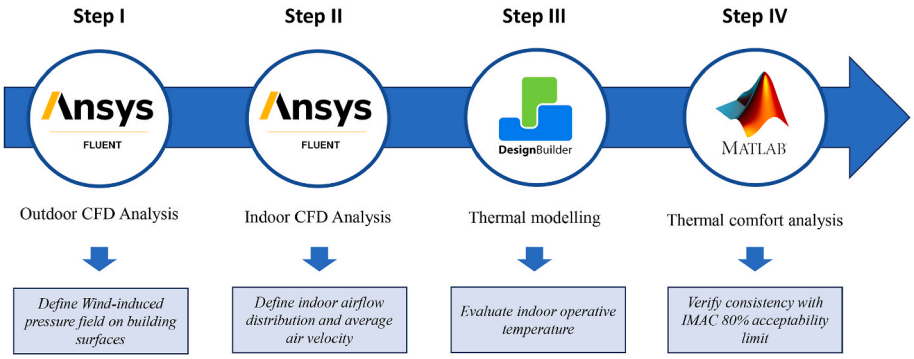

Fig. 4. Methodology flowchart.

typical days corresponding to the three seasons identified by the Indian Meteorological Department for Mumbai. Finally, the values of the three typical days' operative temperatures were compared in Matlab with the acceptability limits provided by the Indian Model for adaptive comfort by evaluating two long-term discomfort indexes.

3.1. Step 1: outdoor CFD analysis

3.1.1. Computational domain and mesh

The first modelling step considers the CFD Analysis of outdoor wind-induced pressures generated on the building surfaces through a 3D RANS equations simulation with Ansys Fluent 2021 R1. The computational domain is built on a full scale with dimensions of 1296 m × 871 m × 510 m for depth, width and height (Fig. 5). The computational domain size was adopted based on the best practice guidelines elaborated by the Working Group of the Architectural Institute of Japan (AIJ) [111] where H denotes the height of the analysed building equal to 85 m.

The computational domain's upstream and lateral boundaries are situated at a 5 H distance from the building, while the downstream boundary lies 10 H away from the leeward wall. The top boundary is positioned 5 H above the roof, resulting in a blockage ratio of 0.4 %, less than 3 % as recommended.

The computational domain was divided into an unstructured grid comprising a polyhexahedral surface mesh, accomplished using the Fluent Meshing tool within Ansys. The computational mesh was created with finer grid resolution near the ground and the building's surfaces, including its openings.

The resolution gradually increased as it moved towards the domain's boundaries, resulting in a smallest cell size of 0.25 m on building surfaces. By moving away from the building, the cells first grow at a rate of 1.0 near the building, gradually reaching a rate of 1.2 at the boundary area with a maximum cell size of 1.5 m, resulting in a total number of cells of 2,379,766.

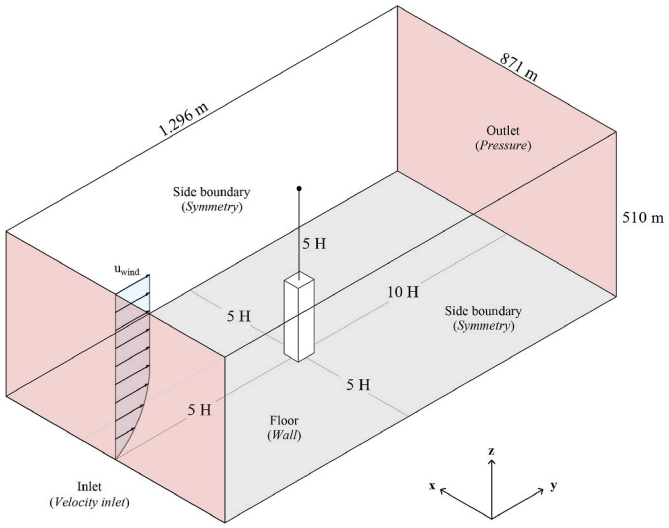

Fig. 5. Computational domain and boundary conditions.

3.1.2. Boundary conditions and solver

In the external CFD simulation, the inlet boundary condition was set as the inlet wind velocity profile. Initially, the Mumbai reference wind velocity from the nearest meteorological station was updated to evaluate the reference site wind speed, considering the varying site roughness attributed to its urban surroundings according to Eq. (1):

$$u_x = \lambda \bullet u_{ref} \bullet \ln\left(\frac{z}{z_0}\right) \tag{1}$$

Where u_x represents the site reference speed at 10 m height, λ roughness coefficient equals 0.25 for high-density urban centres, uref is the reference wind speed at 10 m and z_0 equals 0.05 [m/s].

The wind profile is defined according to the logarithmic law as in Eq. (2), where u^* is the friction velocity, k is the von Karman constant (0.41), and z is the height coordinate.

$$u(z) = \frac{u^*}{k}\left[\ln\left(\frac{z+z_0}{z_0}\right)\right] \tag{2}$$

The value of u^* is determined based on the values of the wind site reference speed (u_x = 2.2 m/s) at reference height (z_{ref} = 10 m) and results equal to 0.504 m/s. Taking into account the urban surrounding of the analysed building, the aerodynamic roughness length (z_0) is set equal to 2.0 m for the city centre.

The turbulence dissipation rate ε is computed with Eq. (3):

$$\varepsilon(z) = \frac{(u^*)^3}{k(z+z_0)} \tag{3}$$

While the specific dissipation rate ω for the SST k-ω model is estimated via Eq. (4):

$$\omega(z) = \frac{\varepsilon(z)}{C_\mu k(z)} \tag{4}$$

where Cμ is an empirical constant taken equal to 0.09.

The building was positioned in the domain perpendicular to the wind action. At the outlet boundary, a zero-static gauge pressure was implemented. The building surfaces and ground employed no-slip boundary conditions, whereas symmetry boundary conditions were applied to the lateral and top boundaries, as shown in Fig. 5. The 3D steady RANS equations were solved in combination with the shear stress transport (SST) k-ω turbulence model. Furthermore, the pressure-velocity coupling algorithm was used, with second-order pressure interpolation and second-order discretization schemes. Convergence was achieved once the scaled residuals plateaued, reaching a minimum of 10^6 for x, y,

and z momentum and 10^4 for k, ω, and continuity.

3.2. Step II: Indoor CFD analysis

3.2.1. Computational domain and mesh

Measured the average pressures on building openings, an indoor CFD analysis on the Type A apartment was performed to assess the three-dimensional distribution of air velocities inside the apartment, using the building's internal volume as a computational domain.

A non-uniform grid approach was used, with increased mesh density surrounding the inlets, outlets, and building walls, while a lower mesh density for the distant field regions. Consequently, the tetrahedral mesh was transformed into a poly hexahedral mesh, enhancing the overall grid quality. To calibrate the CFD analysis results, a grip independency analysis was performed. Three mesh models were analysed: a coarse mesh model with 768,284 cells (M1), a medium-mesh model with 1,536,568 cells (M2), and a fine mesh model with 3,073,136 cells (M3). To assess all areas within the domain, three criteria were considered: the average air velocity along the diagonal line connecting two corners of the domain, the mean air velocity across the entire domain, and the inlet mass flow.

The results of the coarse mesh model deviate to some extent, while the other two models fit well, which indicates that the medium mesh model already has a certain accuracy. The variation between the results obtained using the finer mesh (M3) and the medium mesh (M2) is as follows: 1.7 % for the average air velocity along the diagonal line, 1.1 % for the overall average air velocity, and 0.2 % for the inlet mass flow. These minor discrepancies indicate that the differences between the two mesh models are negligible, affirming the mesh independence of the results. The fine mesh was implemented with an overall number of nodes equal to 10,140,800, a minimum cell size of 0.02 m and a maximum cell size of 0.1 m.

Concerning the computational domain boundary conditions, no-slip boundary conditions and adiabatic boundary conditions were imposed at all walls. The inlet and outlet boundary conditions were set to match the building openings. Pressure boundary conditions were implemented for both inlets and outlets to match the pressures obtained from the Step 1 CFD analysis. The windward openings were considered as inlets, while the leeward ones were as outlets.

In this simulation, as well, the 3D steady RANS equations were solved in conjunction with the shear stress transport (SST) k-ω model. The pressure-velocity coupling employed a coupled algorithm, utilizing second-order pressure interpolation and discretization schemes.

3.3. Step III: Thermal analysis

In Step III, by implementing the indoor ventilation results from the CFD analysis into the building thermal model, a dynamic thermal simulation was performed hourly using DesignBuilder software [116]. The apartment was rebuilt in the geometric model by dividing the various dwellings into different thermal zones according to their intended use. The climate file Mumbai ISHRAE in the *Energyplus* archive was used as the climate file.

Concerning the envelope characteristics for the simulation, the external walls are predominantly made of non-insulated reinforced concrete, the floors consist of a composite structure of concrete and non-insulated brick, and a single-glazed window (SHGC = 0.819) with a wooden frame was assumed. Specifically, a thermal transmittance of 2.54 W/m^{2}K was used for the external walls, 1.92 W/m^{2}K for the intermediate floors and 5.70 W/m^{2}K for the window. No window blinds were set up in the simulation, as they were not in the original design.

As the free-running behaviour of the building was only studied under the effect of natural ventilation, no mechanical systems were used. The thermal simulation was performed for three typical days according to the meteorological seasons identified by the Indian Meteorological Department: the winter season from December to March, the summer season from April to June and the monsoon and pre-monsoon season from July to November.

Specifically, the analysis was carried out on the hottest day of the TMY year, April 5th, characterised by a maximum external temperature of 38.3 °C and a minimum of 25.2 °C, for the summer period, on September 8th, characterised by a maximum temperature of 29.3 °C and a minimum of 24.9 °C, for the monsoon period and on January 13th for the winter period with a maximum temperature of 33.2 °C and a minimum of 17.5 °C. The temperature excursion between day and night on the three analysed days equals 13.2 °C for April 5th, 4.4 °C for September 8th and 15.7 °C for January 13th.

To compare the effectiveness of natural ventilation on indoor thermal comfort, four different ventilation scenarios were considered. The first scenario, named below as WD0, evaluates the thermal building behaviour without natural ventilation driven by the wind action (ACH = 0); the second scenario (WD1) examines the presence of air changes per hour (ACH) of 0.5 h^{-1}, the minimum value required for indoor air quality in residential buildings according to ANSI/ASHRAE 55:2020; the third scenario (WD2) studies the behaviour of the building with an ACH equal to 12 h^{-1}, a typical value in naturally ventilated buildings [112, 113], finally the last scenario (WD3) analyses the ACH driven by cross-ventilation as measured in the CFD analysis with site average velocity wind speed and prevalent direction. Specifically, the average wind speed and prevailing wind direction according to the site wind map were used to assess the typical natural airflow conditions under the most frequent occurrence.

To prevent the adverse effects of indoor overheating resulting from NV during the hottest hours of the day, an operating schedule for the openings was devised. This operative mode is designed to curtail the total opening area dynamically, contingent upon the external temperature, thereby effectively regulating the overall air exchange rate. Fig. 6 shows the percentage of overall ACH used for natural airflow for scenarios WD2 and WD3 according to outdoor temperature in the three analysed days.

Airflow distribution within the dwelling's thermal zones, as measured in the CFD analysis, was set in the thermal simulation using the Interzone airflow tool in DesignBuilder. Except for the natural ventilation characteristics, the occupancy, envelope properties, internal loads and operation schedules of the openings were kept constant. Based on the number of beds in the house, the simulation was based on a total occupancy of seven people. Scheduled daily occupancy and internal heat gain for the different thermal zones used in the simulation are summarized in Table 2. LED lamps with a normalised power density of 2.5 W/m^2 100 lux were provided.

To account for the different average air velocities in the ventilation scenarios, the operative temperature was calculated using ASHRAE Standard 55: 2020 [114] as Eq. (5):

$$t_o = At_a + (1 - A)\bar{t}_r \tag{5}$$

Where t_o is the operative temperature, t_a is the average air temperature, t_r is the mean radiant temperature, and A is a coefficient selected as a function of the relative air velocity v_r ranging from 0.5 ($v_r < 0.2$ m/s), 0.6 ($0.2 < v_r < 0.6$ m/s) and 0.7 ($v_r > 0.6$ m/s).

3.4. Step IV: Thermal comfort assessment

The last step evaluates the consistency of the indoor operative temperatures for each scenario to the indoor thermal comfort limits. Among the different worldwide formulations of the adaptive model, including

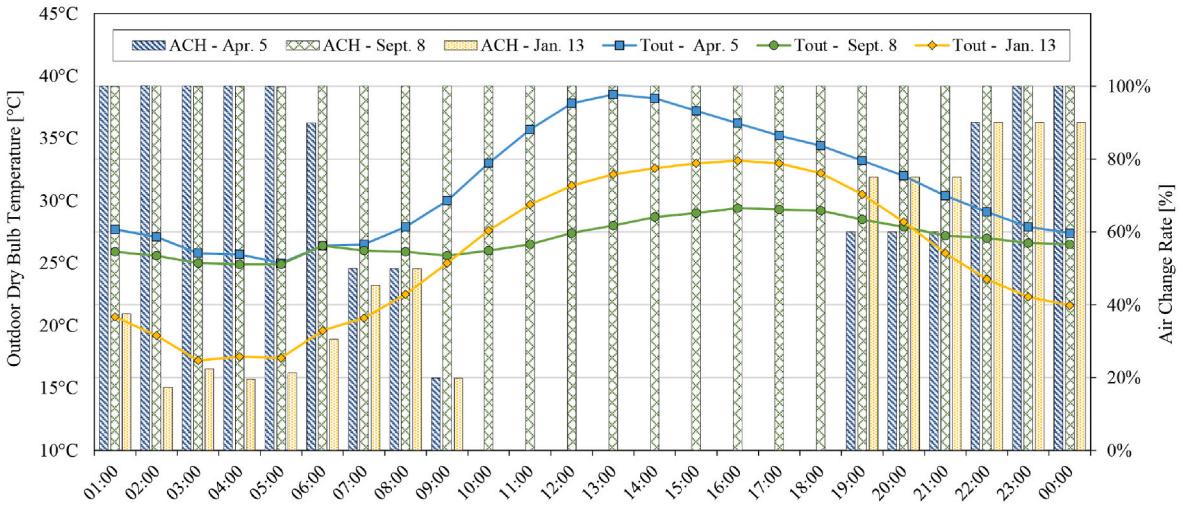

Fig. 6. Daily ACH variability according to outdoor climatic conditions for WD2 and WD3 simulations.

Table 2
Scheduled daily occupancy and internal heat gain for each room.

	Level	N. of people	Occupancy daily time	Appliances and occupancy load [W/m^2][a]
Master Bedroom	Up	2	from 10 p.m. to 8 a.m.	2.67
Double bedroom	Up	2	from 10 p.m. to 8 a.m.	2.67
Double bedroom	Lo	2	from 10 p.m. to 8 a.m.	2.67
Service room	Lo	1	from 10 p.m. to 6 a.m.	2.67
Living room-Dining room	Lo	6	from 8 a.m. to 12 a.m., from 1 p.m. to 2 p.m. from 6 p.m. to 10 p.m.	9
Kitchen	Lo	1	from 7 a.m. to 9 a.m. from 12 p.m. to 2 p.m. from 8 p.m. to 10 p.m.	9
Office room	Lo	1	from 9 a.m. to 12 a.m. from 2 p.m. to 6 p.m.	2.67

[a] According to EN ISO 13790.

Table 3
Airflow characteristics for the analysed ventilation scenarios.

Scenario	Volume	Average Airspeed	Max air speed	Air flow rate	Air change per hour
	V	u_m	u_{max}	q_v	ACH
	[m^3]	[m/s]	[m/s]	[m^3/s]	[h^{-1}]
WD1	675	0.02	0.05	0.10	0.5
WD2		0.19	1.15	2.25	12.0
WD3		0.83	4.39	12.60	67.2

the ones proposed by ASHRAE-55:2020 and EN Standard 16798:2019 [115,116], an adaptive model modified explicitly for the Indian climate called IMAC (India model for adaptive comfort) introduced by Manu et al. [117] and applied in several studies on the assessment of comfort in naturally ventilated buildings in India [118,119] was adopted.

The IMAC model represents an adaptation of the adaptive model proposed by ANSI/ASHRAE-55 modified on real data from buildings located in India and considers the different cultural and climatic contexts of India compared to the assumptions of the ANSI/ASHRAE model mainly developed on data from buildings belonging to temperate/cold climates.

It was, in fact, experimentally found that the comfort standards of the Indian population have higher limits of perceived comfort than the predictions offered by the ANSI/ASHRAE-55 and EN 16798 models. Equation (6) presents the mathematical expression provided by the model for calculating the neutral temperature, as well as the upper and lower 80 % and 90 % acceptability limits compared to ANSI/ASHRAE-55.

IMAC (Indian Model for Adaptive Comfort) ANSI/ASHRAE-55

$$\begin{cases} Upper\,80\%\,acceptability\,limit\,(^{\circ}C) \\ =0.54(T_{out-30DRM})+16.93 \\ Upper\,90\%\,acceptability\,limit\,(^{\circ}C) \\ =0.54(T_{out-30DRM})+15.23 \\ Neutral\,comfort\,temperature\,(^{\circ}C) \\ =0.54(T_{out-30DRM})+12.83 \\ Lower\,90\%\,acceptability\,limit\,(^{\circ}C) \\ =0.54(T_{out-30DRM})+10.43 \\ Lower\,80\%\,acceptability\,limit\,(^{\circ}C) \\ =0.54(T_{out-30DRM})+8.73 \end{cases} \quad \begin{cases} Upper\,80\%\,acceptability\,limit\,(^{\circ}C) \\ =0.31(T_{out-30DRM})+21.3 \\ Upper\,90\%\,acceptability\,limit\,(^{\circ}C) \\ =0.31(T_{out-30DRM})+20.3 \\ Neutral\,comfort\,temperature\,(^{\circ}C) \\ =0.31(T_{out-30DRM})+17.8 \\ Lower\,90\%\,acceptability\,limit\,(^{\circ}C) \\ =0.31(T_{out-30DRM})+15.3 \\ Lower\,80\%\,acceptability\,limit\,(^{\circ}C) \\ =0.31(T_{out-30DRM})+14.3 \end{cases} \tag{6}$$

The $T_{out\text{-}30DRM}$ represents the 30-day running mean outdoor temperature T_{out} calculated as follows with $\alpha = 0.8$:

$$T_{out-30DRM} = (1-\alpha)\left[t_{out(d-1)} + \alpha\left(t_{out(d-2)}\right) + \alpha^2\left(t_{out(d-3)}\right) + \ldots\right] \tag{7}$$

To compare the different scenarios, two long-term comfort indexes were evaluated. Specifically, the POR (Percentage Outside the Range) index, which indicates the percentage of hours in which the operative temperature is outside the acceptable range predicted by the adaptive

model, and the LPD (Long-term Percentage of Dissatisfied) based on the ALD (ASHRAE Likelihood of Dissatisfied), which evaluates how much the indoor operative temperatures deviate from the neutral temperature were assessed [120,121]. The POR, introduced by ISO 7730, requires calculating the percentage of occupancy hours (h_i) in which the operative temperature is outside a specified comfort range relative to the chosen comfort category as follows:

$$POR = \frac{\sum_{i=1}^{Oh}(wf_i \bullet h_i)}{\sum_{i=1}^{Oh} h_i} \tag{8}$$

where w_f is a weighting factor depending on the chosen comfort range.

When referring to the adaptive model, the comfort interval is expressed in terms of operative temperature and the index is denoted $POR_{Adaptive}$. Its formulation follows the Eq. (9):

$$POR_{Adaptive} \propto \begin{pmatrix} wf_i = 1 & \Leftarrow \left(T_{op,in} < T_{op,lower\ limit}\right) \bigvee \left(T_{op,in} > T_{op,upper\ limit}\right) \\ wf_i = 0 & \Leftarrow \left(T_{op,lower\ limit} \le T_{op,in} \le T_{op,upper\ limit}\right) \end{pmatrix} \tag{9}$$

The LPD aims to assess the probability of an uncomfortable phenomenon occurring under certain indoor conditions and to evaluate thermal stress phenomena. LPD index is calculated as follows (Eq. (10)):

$$LPD(LD) = \frac{\sum_{t=1}^{T}\sum_{z=1}^{Z}\left(p_{z,t} \bullet LD_{z,t} \bullet h_t\right)}{\sum_{t=1}^{T}\sum_{z=1}^{Z}\left(p_{z,t} \bullet h_t\right)} \tag{10}$$

where t is the counter for the time step of the calculation period, T is the last progressive time step of the calculation period, z is the counter for the zones of a building, Z is the total number of the zones, $p_{z,t}$ is the zone occupation rate at a certain time step, $LD_{z,t}$ is the Likelihood of dissatisfied inside a certain zone at a certain time step and h_t is the duration of a calculation time step (e.g., 1 h).

The formulation of the Likelihood of dissatisfaction can vary based on the specific reference comfort model used. Among those in the literature [122], the ALD index (ASHRAE Likelihood of Dissatisfied) was used, which is defined in Eq. (11):

$$ALD\left(\Delta T_{op}\right) = PPD(\Delta T_{op}) = \frac{e^{-3.057+0.419\Delta T_{op}+0.007\Delta T_{op}^2}}{1+e^{-3.057+0.419\Delta T_{op}+0.007\Delta T_{op}^2}} \tag{11}$$

where ΔT_{op} is the difference between the indoor operative temperature and the neutral temperature according to the adaptive comfort model. In the analysis, the upper and lower limits of 80 % acceptability predicted by the IMAC model were used as limit values in the calculation of these indexes.

4. Results and discussion

4.1. Outdoor CFD analysis

The first CFD simulation was carried out to assess the wind effects on the building surfaces. Fig. 7 shows the building's influence on the wind flow and summarises its aerodynamic behaviour. As the wind approaches the building, it experiences a slowdown in speed, which comes to a standstill in contact with the building façade. According to the log law wind profile, the wind speed varies from 0 m/s at ground level up to 4.5 m/s at the building's top edge.

Two vortex zones are created, one upwind at the base of the building and a recirculating vortex at the rear due to the shadow zone created by the building as a function of its height. Near the building, the boundary layer detaches, and the laminar becomes turbulent, causing fluid-dynamic instability.

This phenomenon modifies the atmospheric pressure field around the building, transforming the kinetic energy of the airflow into potential energy in the form of a pressure differential. A higher pressure (overpressure) than the ambient atmospheric pressure is created in the upwind zone, the one facing North-West. In comparison, a lower pressure than the atmospheric pressure (depression) is recorded in the leeward zone and on the roof of the building (Fig. 8). Fig. 9a shows the pressure distribution upstream of the windward façade (y = 0 m) on three different vertical lines: at the outer edge of the building (x = 0 m), at one-quarter of the upwind façade of the building (x = 5.5 m) and half of the upwind façade (x = 10.5 m).

As can be seen, the pressure over the upstream facade strongly increases as the height of the building rises. Pressure also varies in the plane, reaching maximum values in the building centre and decreasing symmetrically towards the edges. In the middle of the windward building façade, the maximum values of overpressure are recorded, varying between 4.20 Pa in the lower zone and 11.73 Pa in the upper zone. Approaching the edge, the pressures decrease to become negative at the roof's edge.

On the leeward side (Fig. 9b), facing the southeast, a depression is recorded with greater values in the lowest part of the building. At the half length of the downwind façade (x = 10.5 m), a maximum depression equal to 4.70 Pa is reached; as the height of the building increases, lower values are achieved until reaching the edge of the roof, where the depression begins to grow once more.

The façades in North-East and South-West, parallel to the direction of the wind, present symmetrical pressure values and are characterised by negative pressures. As revealed by the CFD analysis, on the windward

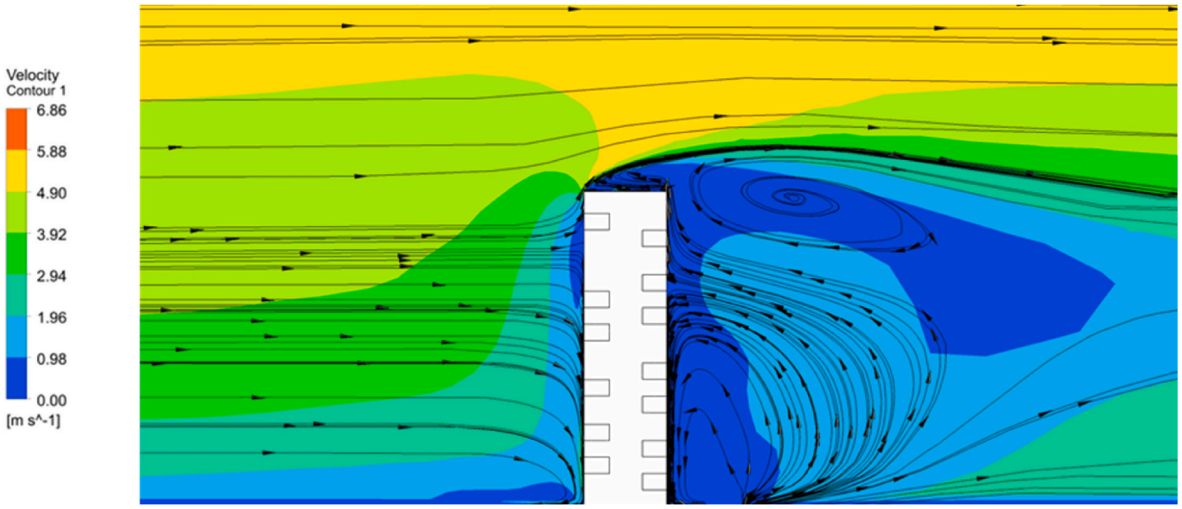

Fig. 7. Wind velocity streamline at the cross-section of Kanchanjunga Apartments.

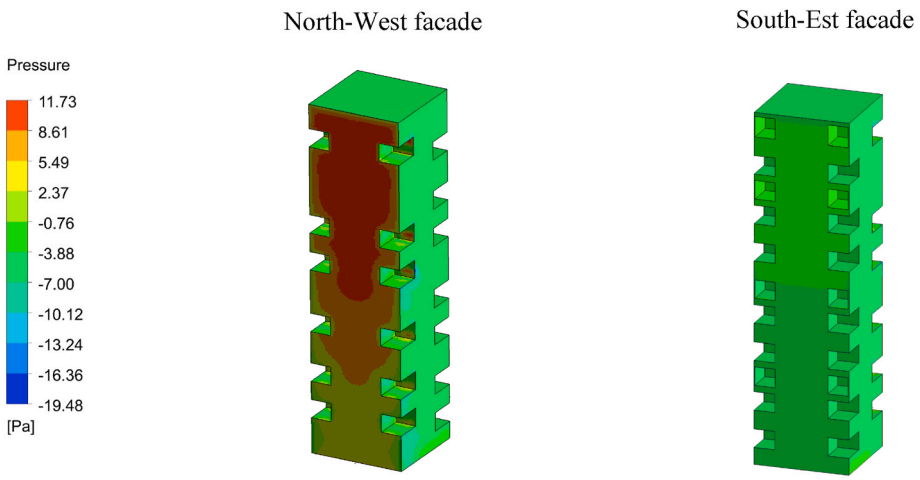

Fig. 8. Wind-induced pressures on building façades.

and leeward building sides, a marked pressure difference that can supply cross-ventilation inside the building, is recorded. Hence, most of the openings in the building were located on these two sides to capitalise on the natural behaviour promoted by wind action and building morphology.

The wind-induced pressure distribution on the surface of the building openings, determined through CFD analysis, is employed as boundary conditions for evaluating indoor ventilation. The average pressure values reached on Type A apartment openings at 35 m above the ground level are shown in Fig. 10.

4.2. Indoor natural ventilation assessment

The distribution of airflow velocity and velocity streamlines in the dwelling are shown in Fig. 11. The air velocity values within the building are normalised by dividing them by the reference site wind speed u_{ref}, resulting in a dimensionless parameter named k, as shown in Eq. (12).

$$k = \frac{u}{u_{ref}} \; [-] \tag{12}$$

The spatial layout of indoor spaces enhances the airflow pattern within the building. This allows for the airflow to move from the side directly facing the wind to the opposite leeward side, thereby improving cross-ventilation (Fig. 11). Horizontal and vertical connections between several building rooms prevent the creation of physical resistance to airflow path, ensuring proper indoor ventilation.

Focusing on the velocity streamlines, wind-induced cross-ventilation is evenly distributed over the entire dwelling. The impact of proper indoor ventilation through placement of air inlets and outlets on opposite sides is apparent. Due to the absence of any openings on sides parallel to the prevalent wind direction, the incoming air experiences no deflection over the length of the building. Consequently, the air reaches significant velocities up to its ends.

A 0.38 average k-value is reached in the dwelling, with peaks near 2.0 achieved at the narrowing of stairways where the airflow section strongly decreases. Higher k-values are achieved at the inlet, peaking at 1.68 in the centre of the smallest opening on the windward side. As the depth of the apartment increases, the k-values decrease. The double-height living room exhibits a maximum k-value of 1.42 at mid-height, with outlet opening k-values reaching 0.70 and 0.72 at the upper and lower floors respectively. Inlet and outlet openings achieve average k-values of 0.82 and 0.28 respectively.

Through CFD building section analysis (Fig. 12), the key elements in this building to ensure proper ventilation can be easily identified. By placing verandas on the windward side, the inlet opening surfaces are reduced, which decreases the effective opening area available for airflow. This effect is opposed on the leeward side by increasing the total outlet opening area with a double-height terrace, resulting in an inlet/outlet ratio of 0.28.

To achieve optimal airflow in the dwelling, a gradual increase in permeability is arranged by modifying section and indoor opening heights. The flow inlet and outlet openings are placed opposite each other, and the elements obstructing the path of air movement are reduced to a minimum, allowing the air to pass freely from the windward side to the leeward one. The double-height living area, located at one-third of the dwelling's length, plays a crucial role in distributing airflow throughout the building. It connects the windward and leeward sides, and thanks to the horizontal floor's subsequent positioning between the two-unit levels, airflow is distributed evenly. To let the air flow through, the double-height core is equipped with indoor openings that allow communication between the two areas of the unit. The layout of the indoor spaces is ensured by the different heights of the horizontal levels, allowing the spaces to be interconnected. Vertical and horizontal connections, such as stairwells, enable the communication between the windward and leeward sides of the building, facilitating the effective performance of natural cross-ventilation. The narrowing of the staircases section, compared to the width of the other room, increases the speed of air movement, producing an acceleration of the airflow along the length of the building till its end.

Under the site's typical wind conditions, the total cross-ventilation airflow reached in the dwelling is 12.6 m^3/s, with 5.2 m^3/s exiting from the upper floor (42 % of inlet airflow) and 7.3 m^3/s from the lower one (58 % of inlet airflow). Within the floors, higher values of airflow rate are concentrated in the area towards the centre of the building, where most of the occupied rooms are placed.

Fig. 13 shows the 3D distribution cross-ventilation airflow according to three analysed ventilation scenarios: scenario WD1 examines the presence of air changes per hour (ACH) of 0.5 h^{-1}, scenario WD2 studies the building behaviour with an ACH equal to 12 h^{-1}, while last scenario (WD3) analyses the ACH driven by cross-ventilation as measured in the CFD analysis with site average wind speed.

The airflow properties achieved by the different ventilation scenarios via CFD simulations are shown in Table 3. An average air speed of 0.83 m/s, 0.19 m/s and 0.02 m/s are achieved by WD3, WD2 and WD1, respectively. WD3 scenario reaches a maximum air speed of 4.4 m/s, WD2 of 1.2 m/s and WD1 of 0.05 m/s. Nevertheless, under the site average wind speed evaluation, too high air indoor velocity for indoor comfort [114] is locally experienced. Therefore, a lower ACH would be more beneficial to prevent the negative effects of draughts.

Table 4 shows the airflow rate values for all openings used to simulate the thermal performance of the building under cross-

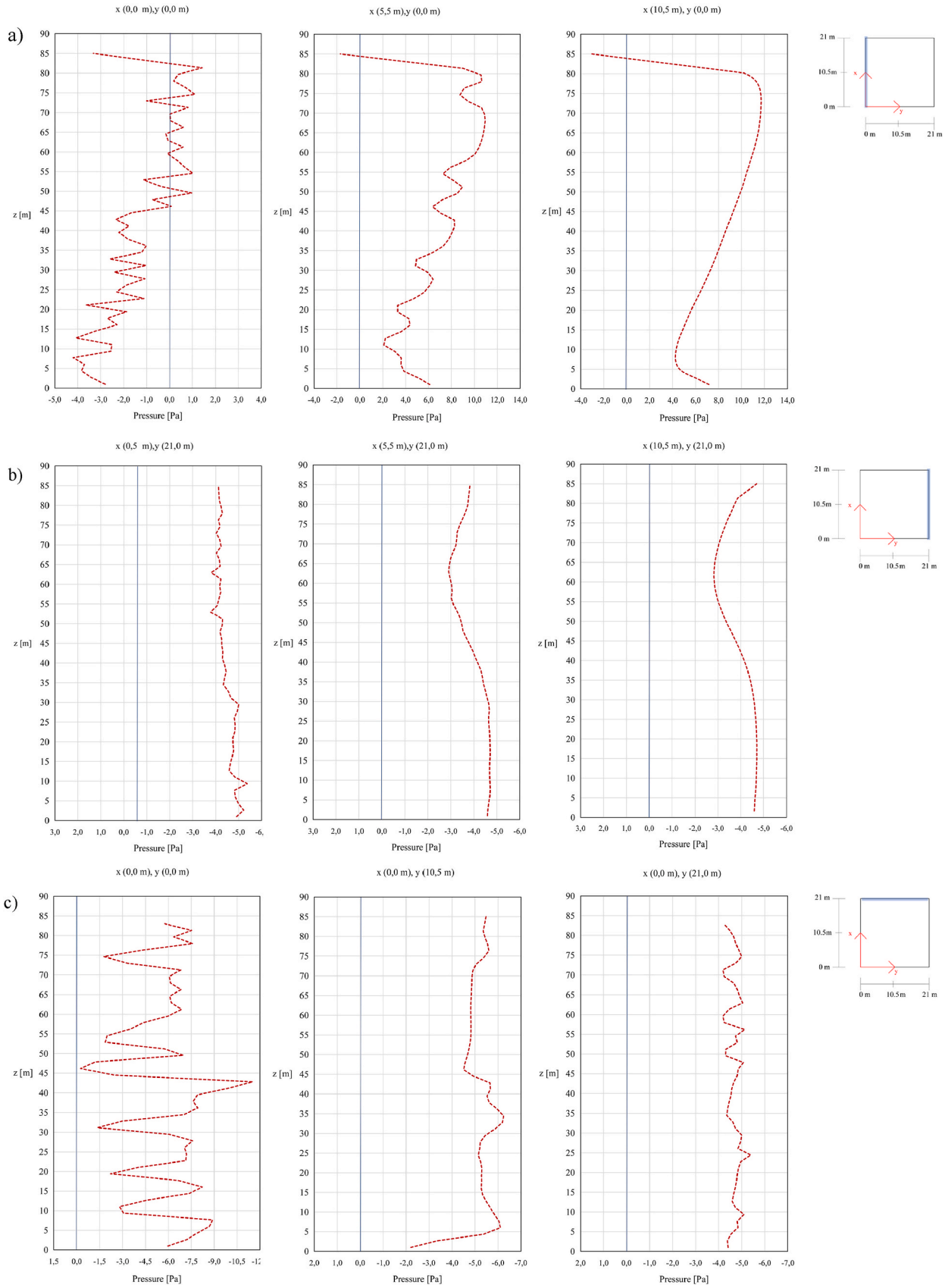

Fig. 9. Wind-induced pressure values on building surfaces: a) windward side (x = 0; 5.25; 10.5 m and y = 0 m), b) leeward side (x = 0; 5.25; 10.5 m and y = 21 m), c) wind parallel side (x = 0 m and y = 0; 10.5; 21 m).

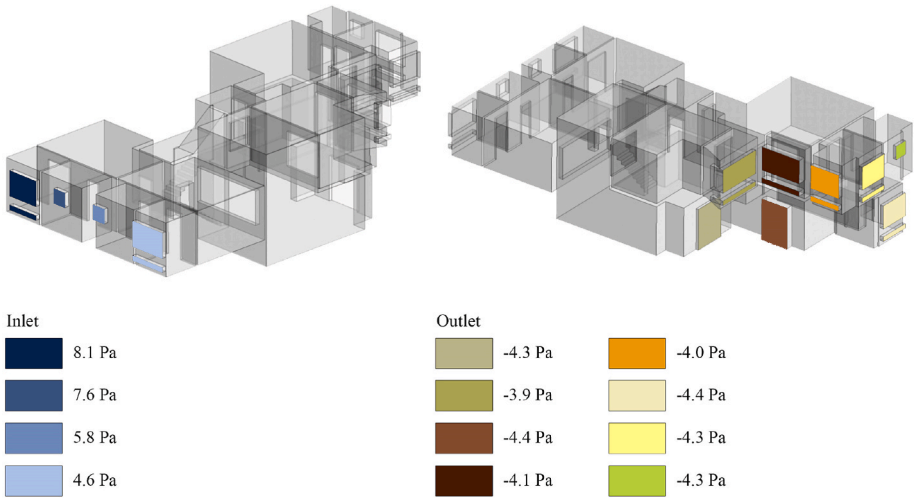

Fig. 10. Average wind-induced pressures on Type A apartment openings at 35 m above ground level.

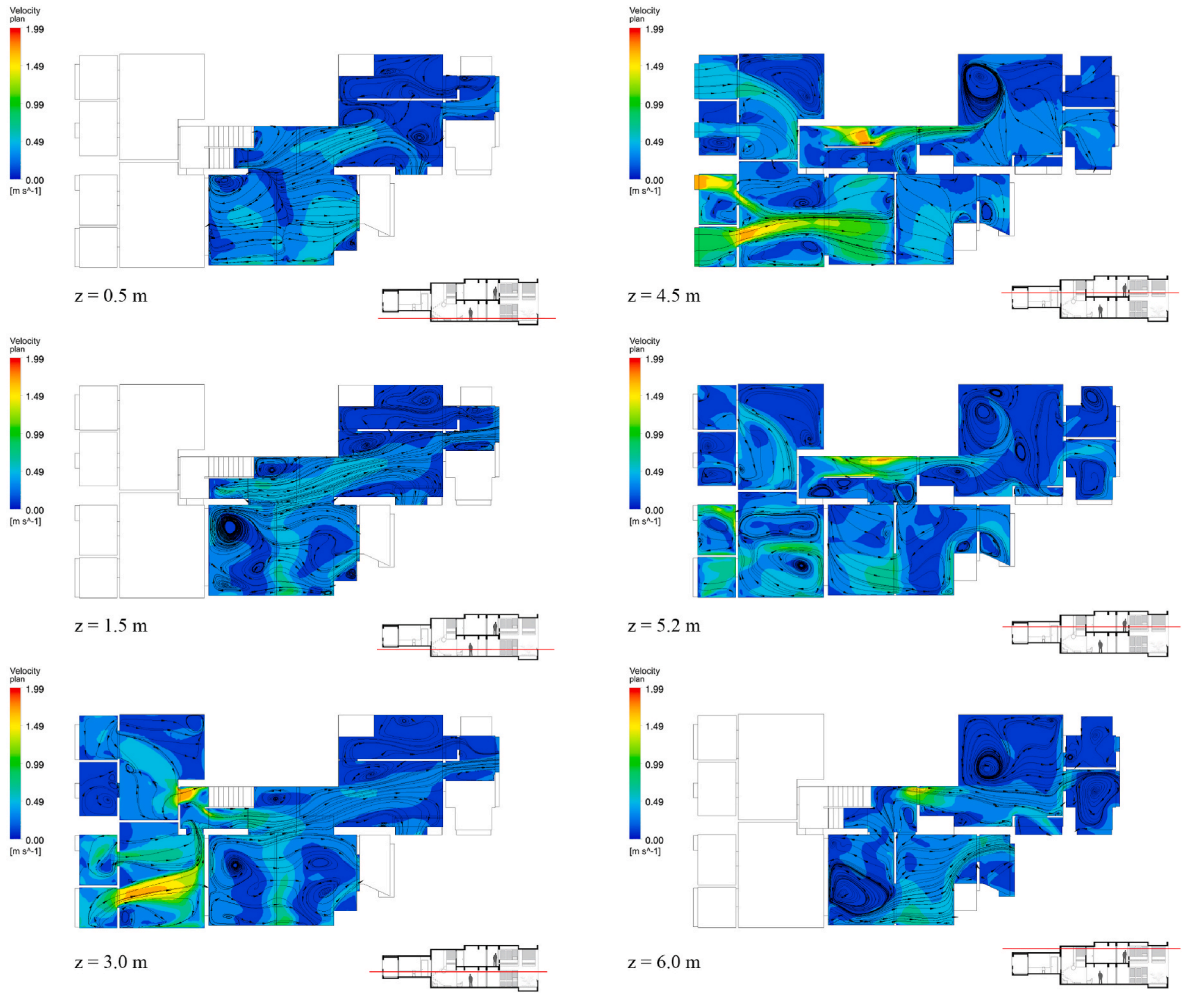

Fig. 11. Air velocity and velocity streamlines on the horizontal plane in Type A apartment at different heights (z = 0.5 m, z = 1.5 m, z = 3.0 m, z = 4.5 m; z = 5.2 m and z = 6.0 m) from the lower floor.

ventilation effect via multi-zone circuit model: openings are represented as resistances (R), while rooms are represented as nodes. Subscripts indicate where the airflow comes from and goes to: “i" and “o" indicate the inlet from the outside and the outlet to the outside, while the numbers indicate the different rooms. Fig. 14 shows the schemes of resistances and nodes in the dwelling.

4.3. Indoor thermal analysis

The natural ventilation properties achieved by the different

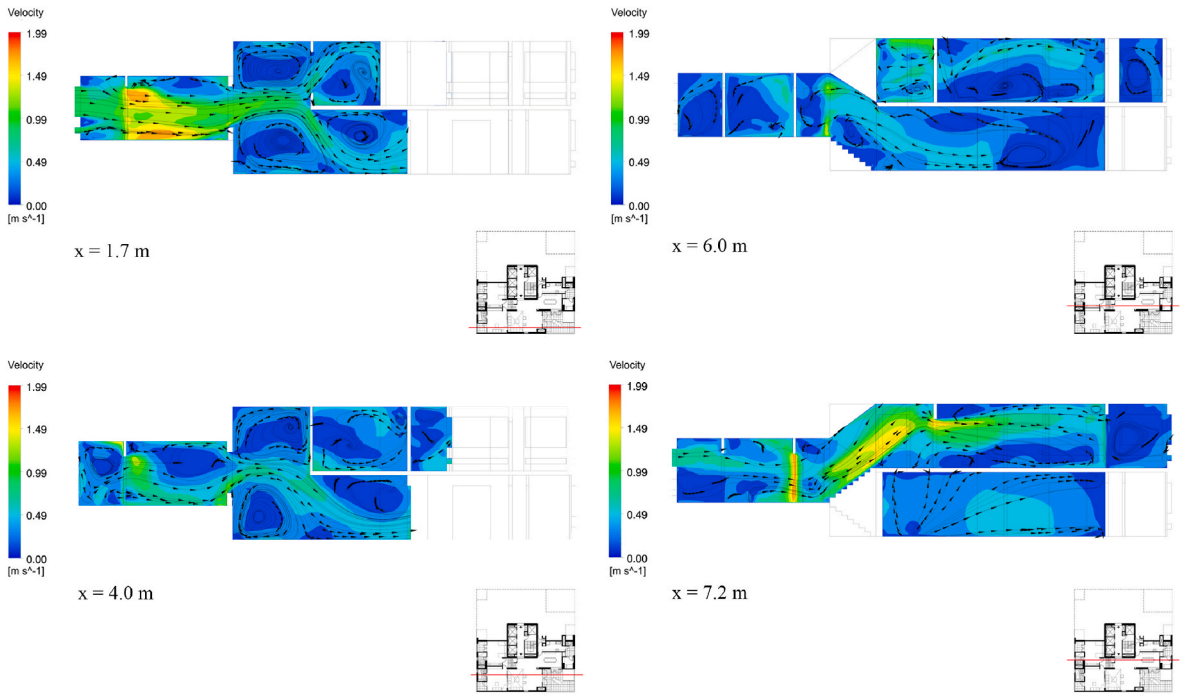

Fig. 12. Air velocity and velocity streamlines on the vertical plane in Type A apartment at different quotas (x = 1.7 m, x = 4.0 m, x = 6.0 m and x = 7.2 m) from the building edge.

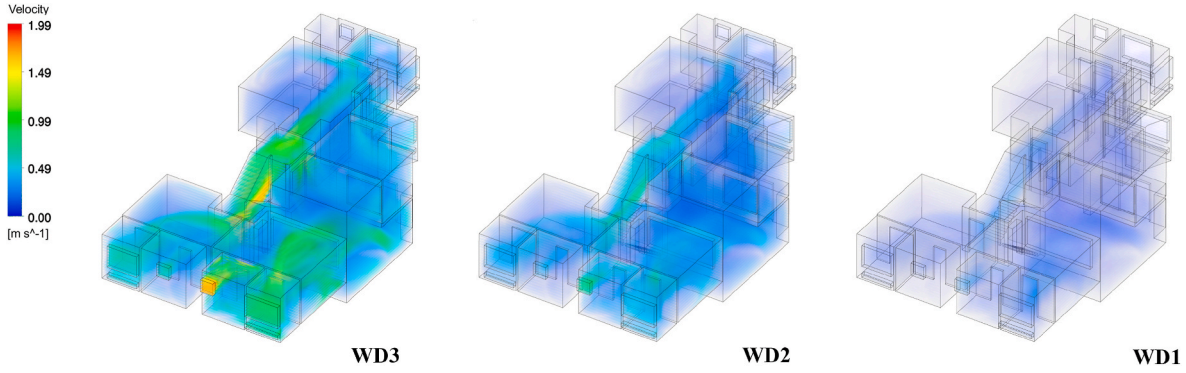

Fig. 13. 3D distribution cross-ventilation airflow according to three ventilation scenarios.

ventilation scenarios in the CFD analysis were implemented in the thermal model to assess the thermal dynamic performance of the dwelling under the cross-ventilation effect.

Fig. 15a shows the operative temperature values for the different ventilation scenarios on April 5th, the hottest day, compared to no ventilation. The analysis clearly shows the influence of natural ventilation, which, thanks to its ventilative cooling potential, significantly reduces indoor operative temperatures. Compared to the scenario without cross-ventilation (WD0), all the scenarios with natural ventilation provide a reduction in indoor operative temperatures that improves with increasing air change rate and increasing average air velocity. The maximum operative temperature difference between the unventilated and ventilated configurations is recorded in the WD3 scenario.

In this scenario, a maximum decrease in operative temperature of 6.5 °C occurs in the early hours of the day (4:00 a.m.) when the building benefits from the structural cooling produced by night ventilation. In comparison, the minimum reduction of 4.0 °C occurs at 7:00 p.m. when the building is affected by the thermal lag of the heat accumulated during the hottest hours of the day.

Scenario WD2 exhibits a maximum operative temperature difference with case WD0 of 5.3 °C and a minimum of 3.1 °C, while scenario WD1 achieves lower reduction values like no-ventilated one. A maximum drop in operative temperature of 0.9 °C and a minimum of 0.5 °C is achieved.

During the daytime hours, when the outdoor temperature reaches its maximum, all scenarios ensure temperatures significantly lower than the outdoor dry bulb temperature with increasing values as the amount of ventilative cooling at night increases. The most marked reduction occurs at 12:00, during the daily temperature peak of 38.3 °C, with values of 3.6 °C in the WD1 scenario, 6.4 °C in the WD2 scenario, and a maximum of 7.6 °C in the WD3 scenario.

As the outdoor temperature difference between the daily maximum and minimum temperatures reduces, the cooling effect of natural ventilation decreases. Nevertheless, as shown in the analysis for September 8th (Fig. 15b), a significant reduction between the operative temperature of the unventilated and the ventilated scenarios is recorded, with an average decrease of 3.5 °C over the day. The maximum drop in operative temperatures is generated by the WD3 scenario with a reduction of 5.8 °C, followed by the WD2 scenario with a decrease of 4.7 °C and finally by the WD1 scenario with 0.7 °C.

Table 4
Airflow rate for each apartment opening according to three analysed ventilation scenarios based on Fig. 14 schematisation.

Lower Floor					Upper floor				
Opening ID	***Opening surface***	***Air flow rate***			***Opening ID***	***Opening surface***	***Air flow rate***		
	[m^2]	[m^3/s]				[m^2]	[m^3/s]		
Scenario		***WD3***	***WD2***	***WD1***	*Scenario*		***WD3***	***WD2***	***WD1***
Ri,1	2.76	3.91	0.70	0.031	**R7,11**	2.82	4.38	0.78	0.035
Ri,2	0.57	0.88	0.16	0.007	**R11,12**	1.91	2.84	0.51	0.023
Ri,3	0.57	2.02	0.36	0.016	**R8,11**	1.78	0.66	0.12	0.005
Ri,4	3.08	5.80	1.04	0.046	**R8,13**	3.55	1.54	0.27	0.012
R1,5	3.30	3.91	0.70	0.031	**R11,13**	1.93	0.87	0.16	0.007
R2,5	1.51	0.88	0.16	0.007	**R13,14**	3.00	2.42	0.43	0.019
R3,6	1.51	2.02	0.36	0.016	**R14,o**	3.76	2.42	0.43	0.019
R4,6	2.16	5.80	1.04	0.046	**R12,o**	3.67	1.34	0.24	0.011
R5,7	1.89	4.79	0.86	0.038	**R12,15**	1.51	0.15	0.03	0.001
R6,7	1.84	1.16	0.21	0.009	**R12,16**	2.33	1.36	0.24	0.011
R6,8	6.91	6.65	1.19	0.053	**R16,o1**	2.79	0.81	0.15	0.006
R7,8	2.82	1.58	0.28	0.012	**R16,o2**	2.74	0.54	0.10	0.004
R8,10	1.90	1.16	0.21	0.009	**R15,o**	0.57	0.15	0.03	0.001
R8,9	1.90	0.16	0.03	0.001					
R8,o2	4.29	3.92	0.70	0.031					
R8,o1	3.75	2.18	0.70	0.031					
R9,10	1.49	0.16	0.03	0.001					
R10,o	2.73	1.31	0.23	0.010					

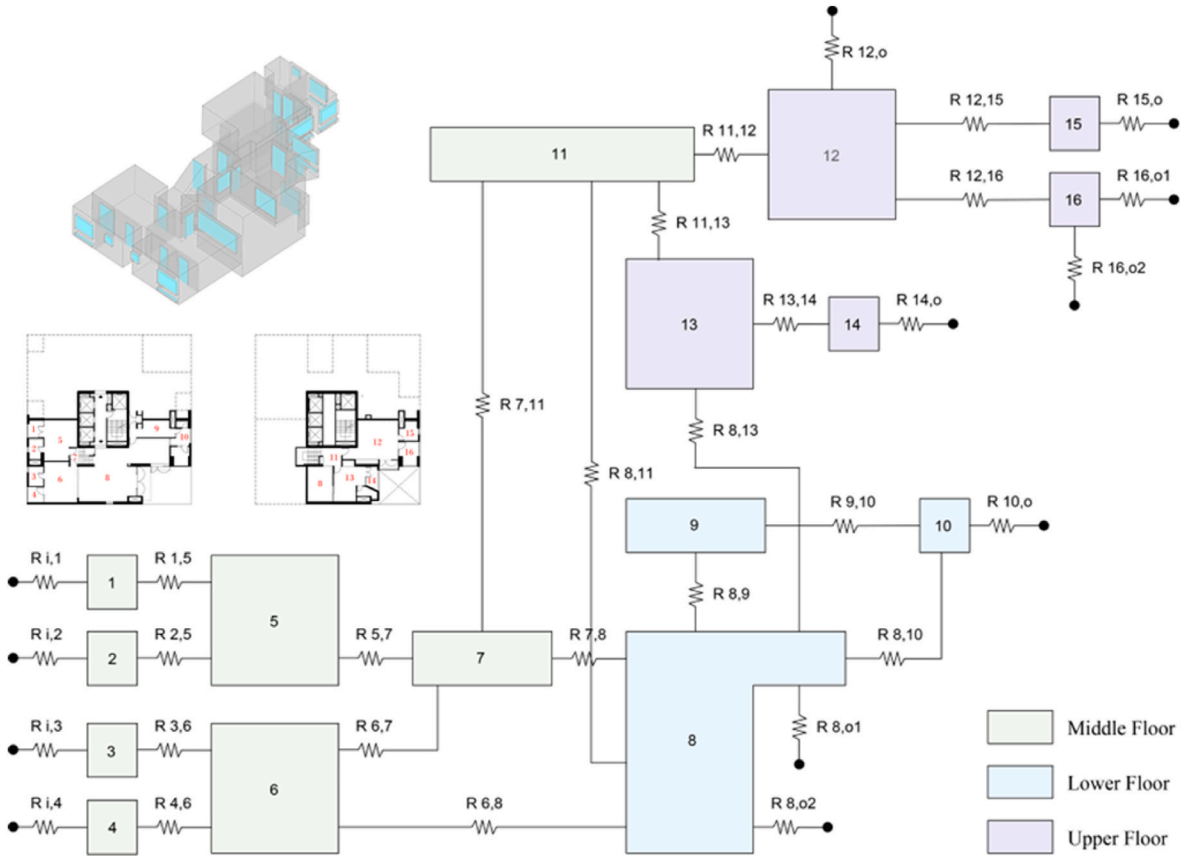

Fig. 14. Scheme of Type A airflow rate using a multi-zones circuit model: openings are represented as resistances while rooms are nodes.

On January 13th, when there is a greater daily temperature fluctuation, the thermal performance of the dwelling is similar to those on the hottest day, as shown in Fig. 15c. Nevertheless, due to the relatively lower minimum outdoor temperatures, the effect of night-time ventilative cooling becomes more evident. Therefore, natural ventilation exhibits increased efficiency in decreasing the maximum operative temperature in all ventilated scenarios when compared to the baseline case. The maximum operative temperature difference, compared to WD0, drops by 1 °C, 6.1 °C and 7.2 °C in WD1, WD2 and WD3 scenario, respectively.

4.4. Thermal comfort assessment

Fig. 16 presents the operative temperature values achieved by the various analysed scenarios compared to the acceptability limits provided by the IMAC comfort model on April 5th, September 8th and

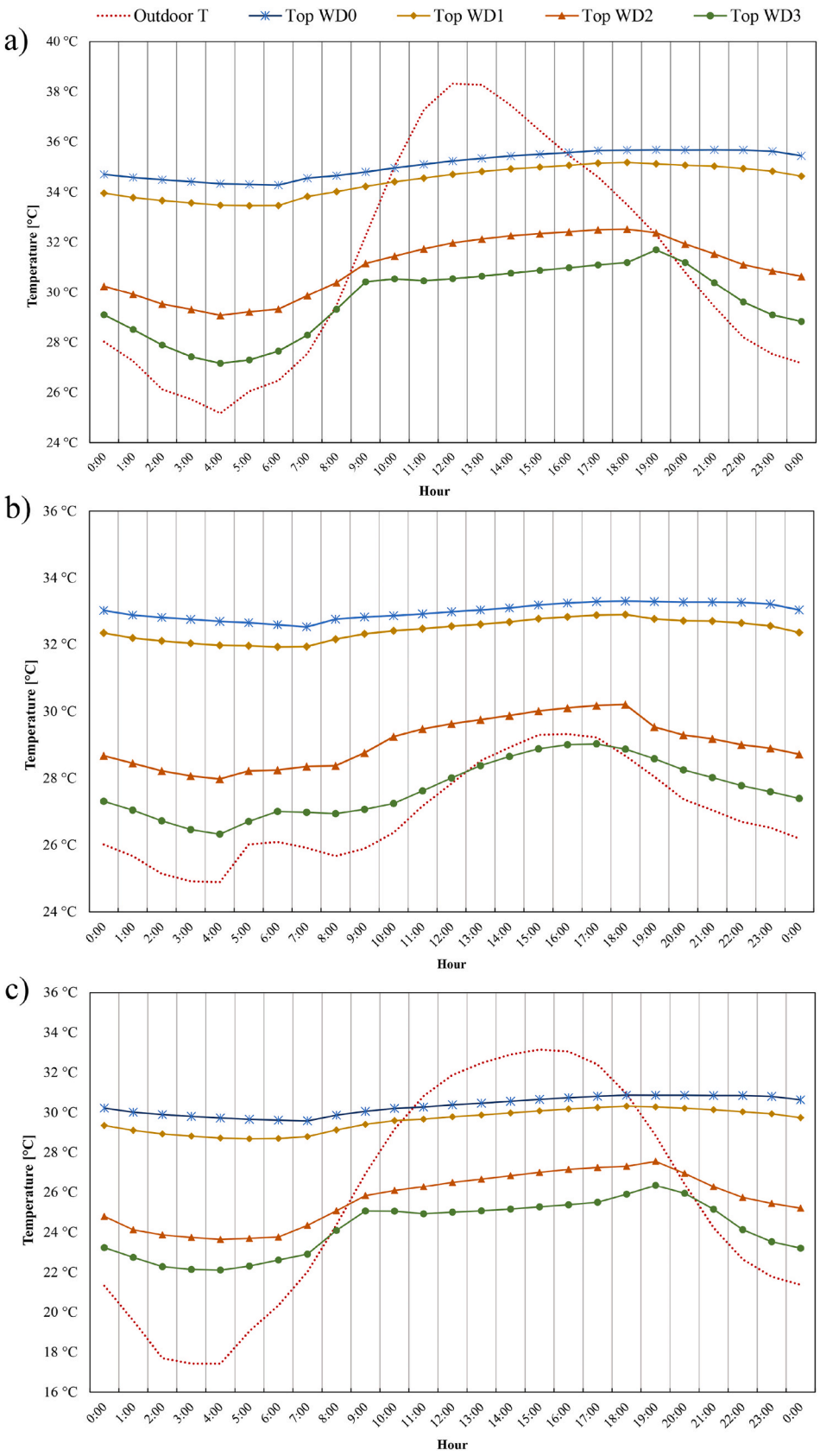

Fig. 15. Operative temperature trend on an hourly basis assessed on a) April 5th, b) September 8th and c) January 13th for the different ventilation scenarios.

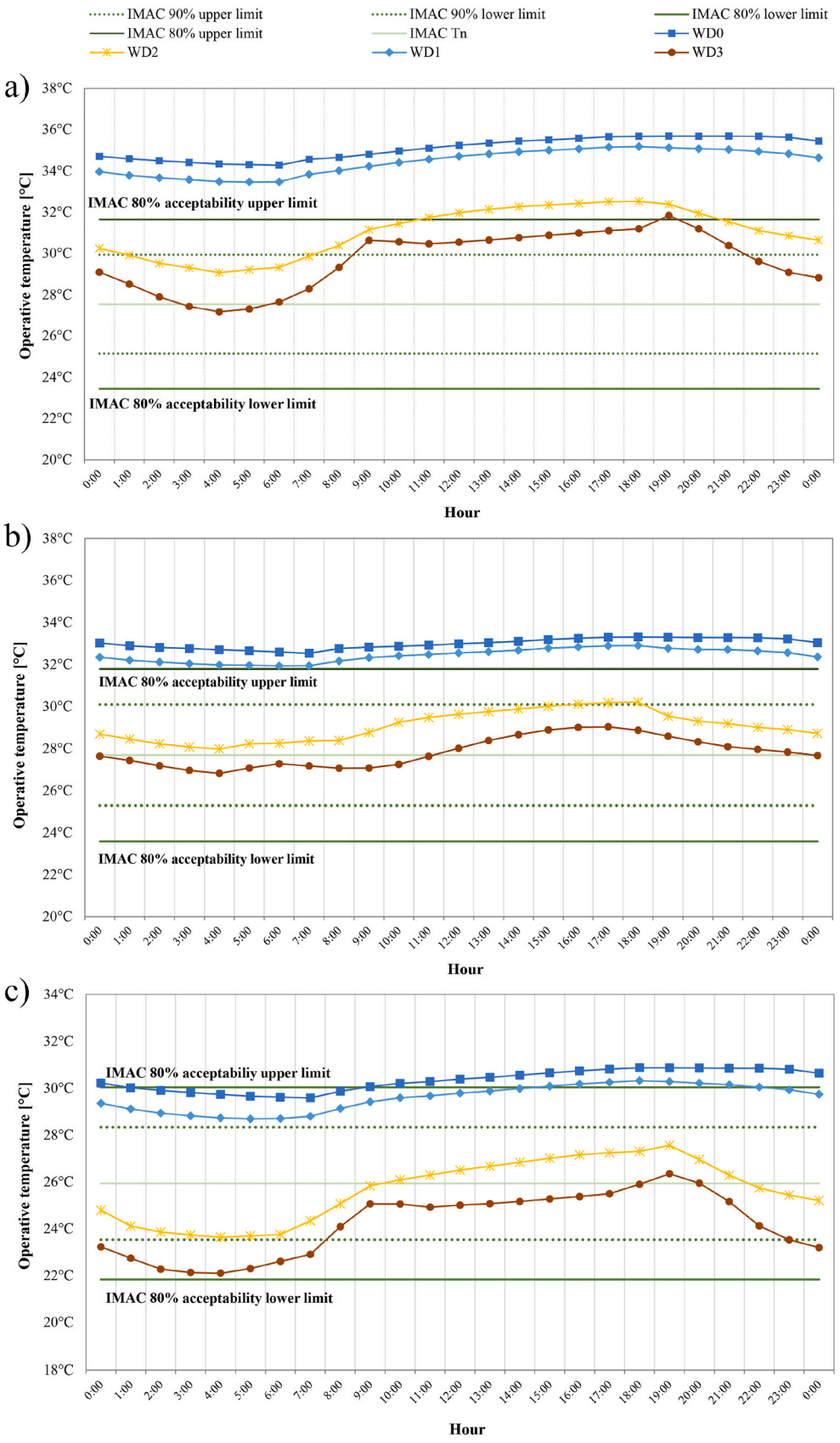

Fig. 16. Thermal comfort assessment on a) April 5th, b) September 8th and c) January 13th according to the IMAC model's acceptability limits.

January 13th. The 30 days-running mean outdoor temperatures ($T_{out-30drm}$) is estimated at 27.2 °C for April 5th, 24.2 °C for January 13th and 27.5 °C for September 8th.

On the hottest day, operative temperatures exceeding the acceptable upper limit of IMAC model are observed throughout the day in scenarios where there is no natural ventilation or minimal air changes per hour. The effectiveness of night-time ventilative cooling becomes evident when air change rates exceed 12 ACH. In the WD2 scenario, comfort limits are met during the early morning and evening hours, while operative temperature values rise significantly during peak daytime heat.

On the other hand, the WD3 scenario, which incorporates natural cross-ventilation based on the site's average reference wind speed, achieves indoor comfort throughout most hours of the day, primarily due to night-time ventilative cooling. This is the case except for 19:00 when the heat accumulated during the hottest hours of the day begins to affect the building. However, reactivating natural ventilation leads to a return of operative temperature values to the acceptable range.

On 8th September, WD2 and WD3 scenarios ensure operative temperatures within acceptable indoor comfort limits for all analysed hours. Conversely, WD0 and WD1 scenarios do not meet these conditions and exceed the acceptability limit. On 13th January, when a more significant daily temperature excursion occurs, WD0 and WD1 scenarios meet the indoor comfort acceptability values only for a limited part of the day. Specifically, the WD0 scenario maintains acceptable values between 1:00 a.m. and 8:00 a.m., while the WD1 scenario extends this interval from 11:00 p.m. to 1:00 p.m. In contrast, the WD2 and WD3 scenarios record operative temperatures within acceptable limits throughout the day. Table 5 shows the POR and LPD index values for the various ventilation scenarios on typical days. On the hottest day, the WD0 and WD1 scenarios indicate a POR value of 100 % for discomfort hours.

Comparatively, the WD2 scenario shows a 58 % reduction in discomfort hours compared to the scenario without ventilation, and the WD3 scenario achieves a more amplified decrease of 96 %, hence yielding a POR value of 4 %. On September 8th, the POR index reaches a full 100 % for both WD0 and WD1 scenarios, but drops to 0 % for WD2 and WD3 scenarios.

This demonstrates how ventilative cooling, thanks to cross-ventilation with an air changes rate higher than 12, generates a 100 % reduction in the number of discomfort hours in the building. Among the simulated days, January 13th exhibits the lowest recorded POR value. In the WD0 scenario, the POR stands at 68 %, while the WD1 scenario records 32 %. On the other hand, the WD2 and WD3 scenarios both yield a POR of 0 % for the hours analysed, resulting in a total 100 % reduction in discomfort hours when compared to the no-ventilated scenario.

Focusing on $LPD_{Adaptive}$ values, as the air changes rate and average air velocity increase, the potential of ventilative cooling in improving thermal comfort conditions increases. The WD3 scenario generates a reduction in the probability of dissatisfaction of 80 % on the hottest day and 81 % on September 8th compared to the scenario without natural ventilation, recording the closest values to thermal neutrality among the different scenarios. On 13th January, the WD2 scenario generates the most substantial reduction of 71 %, in contrast to the scenario without ventilation.

Indeed, the WD3 scenario shows a higher LPD value than the one for the WD2 scenario. Although WD3 represents a solution with values closer to thermal neutrality during the hottest hours, increasing the ventilation flow rates at night, when outside temperatures are lower, produces a more significant downward deviation of operative temperature from thermal neutrality than the values obtained from the WD2 scenario with lower ACH.

Table 5
POR and LPD index values on different days calculated for the different ventilation scenarios.

$POR_{Adaptive}$ *(IMAC 80 %)*				
	WD0	WD1	WD2	WD3
April 5th	100 %	100 %	42 %	4 %
September 8th	100 %	100 %	0 %	0 %
January 13th	68 %	32 %	0 %	0 %
$LPD_{Adaptive}$ $^{<ALD>}$				
	WD0	**WD1**	**WD2**	**WD3**
April 5th	62 %	54 %	20 %	12 %
September 8th	26 %	20 %	8 %	7 %
January 13th	35 %	29 %	7 %	10 %

4.5. Discussion

The findings of the present study demonstrated the ventilative cooling potential of cross-ventilation on thermal comfort for high-rise buildings in a hot and humid climate.

In such climatic conditions, structural cooling through cross-ventilation at night is discovered as a successful approach to decrease the operative temperature on the hottest days, even when the outdoor temperature reaches up to 39 °C. The cooling effect achieved during the night reduced the operative temperature up to 6.5 °C compared to the one without NV. Scenarios with higher air change rates ensure better indoor thermal comfort conditions, especially on days marked by elevated daily thermal excursion. In line with Dhalluinn et al. [123] and Chiesa et al. [11], NV can produce overheating problems in a hot and humid climates. Therefore, increased air exchange through ventilation is advantageous at night. Conversely, during the hottest hours, it is not beneficial, and low or no air flow is preferred. When the temperature is not excessively high, increasing air speed through cross ventilation can reduce occupants' discomfort. It was found that cross-ventilation, increasing airflow velocity, affects the occupants' perception of comfort, whereas night ventilation provides a higher level of comfort in air temperature reduction.

Hence, to fully benefit, the NV operating mode is crucial. Higher air change rates are more beneficial in reducing indoor temperatures, but simultaneously result in a more significant deviation from the neutral temperature during the hottest or coldest hours. At the same time, although the relationship between draught sensation and indoor air velocity at different temperature ranges indicates that the air velocities required by occupants increase with increasing operative temperatures, the WD3 scenario with higher ACH, resulted in a localized peak velocity inside the building that exceeded the acceptable level. Consequently, this solution is unsuitable.

Although several studies [57,124] have demonstrated how, in naturally ventilated buildings, average air velocities of up to 1.5 m/s during the hot season can be tolerated, scenario WD3, even with an average air velocity of 0.83 m/s, achieved localized peaks of up to 4.4 m/s. This finding stresses the importance of the combined use of CFD with BES to precisely evaluate airflow distribution within buildings and identify potential localized discomfort issues.

The cooling potential achieved in the WD3 scenario may, however, provide an interesting application for high-rise office buildings, where, due to different occupancy schedules that generally do not include night-time occupancy, it may represent an effective passive cooling technique.

Moreover, it is also worth noting that the most significant reduction in operative temperature between scenarios occurs between the 0.5 and 12 ACH scenarios. While WD3 had the greatest reduction in operative temperature, a small difference is observed between it and the WD2 scenario on all days examined. When analysing the reduction rate in operative temperature compared to the increase in ACH, it was found that the effectiveness of reducing operative temperature decreases as the air change rate increases.

For example, on the hottest day, when the most significant reduction occurred at 4:00 a.m., the WD1 scenario with 0.5 ACH achieved a drop in operative temperature of 0.85 °C compared to WD0. The reduction rate between 0.5 and 12 ACH (WD2 scenario) attained a value of 0.16 °C

for each 0.5 ACH increase, while between WD2 and WD3, the rate drops dramatically to 0.02 °C for each 0.5 ACH increase. This is mainly due to the reduced cooling potential of outdoor temperatures, given the high average temperatures, and suggests that in other colder climates, increasing ACH may be otherwise beneficial.

The research also points out that in naturally ventilated buildings, occupant adaptation is particularly relevant when assessing thermal comfort acceptability, and the correct choice of comfort model becomes paramount. Conversely to other comfort models ineffective in predicting comfort conditions in hot climates, the IMAC offered a wider range of acceptability limits able to manage the more effective use of NV. Compared to the previous studies [118,125,126], higher reductions in discomfort hours ranging from 96 % to 100 % were achieved, thanks to the cooling potential of cross-ventilation.

This phenomenon is attributable to the impact of building form design on enhancing the potential for cross-ventilation and the correct distribution of airflow within the building, thereby contributing to an improved perception of thermal comfort. The CFD analysis carried out on the examined building proposes noteworthy findings, which have been effective in enhancing the building's natural ventilation. These findings may be suitable for this building typology.

In contrast to the usual spatial layout of high-rise buildings, where multiple apartments on the same floor typically face a single side or, at most, a corner exposition, a more favorable approach entails designing flats that extend along the entire length of the building. This guarantees them dual exposure to the prevailing winds and maximises the pressure difference between the building's facades. Implementing a duplex apartment layout in high-rise buildings, achieved by vertically shifting horizontal floors, has demonstrated to be a successful design strategy to tackle this issue.

The ideal positioning for openings involves placing them primarily on the windward and leeward sides of the building, taking advantage of pressure differentials. To enhance airflow rate within the building, wider openings need to be situated at the center of the windward façade, where the highest overpressure is attained. Furthermore, for improved airflow pathways throughout the building, it is essential to sustain a smaller inlet surface area than on the leeward side, which enhances the air velocity at the inlet. Keeping the inlet-to-outlet ratio at 0.28 is effective in accomplishing a proper free-flow path.

This finding, related to a real case study, confirms what was found by Zhang et al. [86] in the analyses of an ideally cross-ventilated cubic single zone. The study recommended an inlet/outlet ratio of less than 0.5 between the total inlet and outlet area to improve air distribution within the building.

Simultaneously, a growing progression of air permeability, attainable through adjustments in section heights and indoor opening placement and size, proved to be effective in ensuring continuity throughout the building. A double-height space at 1/3 of the building depth provided with indoor openings allows an easier functional indoor layout, ensuring airflow path interconnection between different building levels. Likewise, an open stairwell helps channel the airflow, directing it to other building areas. Further investigations should be carried out to evaluate more in-depth their influence on the airflow distribution by means of comparative analysis.

In addition, future investigations would also look more closely at characterising the effect of wind on natural ventilation. This study assumed that the wind effect is constant in intensity and direction and evaluated the influence of surrounding environments empirically. However, many studies have shown how this can adversely affect ventilation rates [127–129] and how ventilation varies with atmospheric stability [130]. In addition, fluctuations in wind speed and direction, as well as air temperature and humidity, cause the ventilation rate to deviate significantly from its mean value, as assumed in the study [83,131]. Explicit modelling of the building surroundings, varying atmospheric stability, and several wind directions will be useful in future CFD simulations to improve ventilation rate prediction accuracy.

5. Conclusions

Given the evident impacts of climate change, it is undeniable that a re-evaluation of the interaction between buildings and climate is imperative to meet the challenging increase in global cooling energy demand. Adopting the passive principles of bioclimatic architecture and prioritizing the synergy between building design and the environment must once again become central to the building design process, and national policies must be used to promote their use, especially concerning the UN Sustainable Development Goals. Natural passive cooling methods, such as natural ventilation, have the potential to play a crucial role in reducing energy consumption in contemporary building design and in coping with the rising energy poverty, particularly in the Global South.

Wind-induced cross-ventilation has undoubtedly proved to be the most passive and effective ventilation method for buildings, especially if cooling loads are to be reduced. Notwithstanding, the struggling challenge in empowering cross-ventilation potential within the buildings is to ensure spatial continuity between the windward and leeward sides against the indoor spaces' layout needs. This objective turns out to be even more complex when dealing with high-rise buildings, where, due to the high-density building typology, the main design effort is made to maximize the number of apartments available on the same floor.

In this study, the viability of ventilative cooling in an emblematic cross-ventilated post-modernist high-rise building was investigated. With a novel simulation methodological approach across multiple digital environments, the study demonstrates how cross-ventilation can ensure affordable indoor thermal conditions even in adverse climatic conditions like the Indian ones.

The ventilative cooling potential of NV, primarily through night-time structural cooling, achieves notable improvements in indoor comfort conditions. A maximum reduction in operative temperature of up to 5.3 °C compared to the scenario without natural ventilation and up to 6.4 °C compared to the peak outdoor temperature on the hottest day. As daily thermal excursion grows, the ventilative cooling potential of night-time natural ventilation increases, providing a drop in operative temperature up to 6.1 °C compared to no ventilated scenario.

Consistently with IMAC's 80 % acceptability limits, cross-ventilation ensures a reduction of up to 58 % of discomfort hours on the hottest day and a total reduction of discomfort hours on typical monsoon and winter days. The methodology and results of this study are intended to assist architects and policymakers in quantifying the cooling potential of natural ventilation in high-rise buildings, suggesting alternative passive solutions for cooling energy saving.

Future work will include a more in-depth analysis of local indoor thermal comfort to assess possible localized discomfort due to excessive air velocity. A parametric study evaluating the influence of different opening surfaces and dwelling depths on cross-ventilation potential will be carried out to provide further design guidelines for better indoor ventilation performance in high-rise buildings.

CRediT authorship contribution statement

Roberto Stasi: Writing – review & editing, Writing – original draft, Visualization, Resources, Methodology, Formal analysis, Conceptualization. **Francesco Ruggiero:** Writing – review & editing, Supervision. **Umberto Berardi:** Writing – review & editing, Supervision.

Declaration of competing interest

The authors declare that they have no known competing financial interests or personal relationships that could have appeared to influence the work reported in this paper.

Data availability

Data will be made available on request.

References

[1] J. Hansen, R. Ruedy, M. Sato, K. Lo, World of change: global temperatures, Rev. Geophys. 48 (2020), https://doi.org/10.1029/2010RG000345/ABSTRACT.

[2] A. Dimitrova, V. Ingole, X. Basagaña, O. Ranzani, C. Milà, J. Ballester, C. Tonne, Association between ambient temperature and heat waves with mortality in South Asia: systematic review and meta-analysis, Environ. Int. 146 (2021), 106170, https://doi.org/10.1016/J.ENVINT.2020.106170.

[3] V. Pérez-Andreu, C. Aparicio-Fernández, A. Martínez-Ibernón, J.L. Vivancos, Impact of climate change on heating and cooling energy demand in a residential building in a Mediterranean climate, Energy 165 (2018) 63–74, https://doi.org/10.1016/j.energy.2018.09.015.

[4] M. Santamouris, Cooling the buildings – past, present and future, Energy Build. 128 (2016) 617–638, https://doi.org/10.1016/j.enbuild.2016.07.034.

[5] B. Bandyopadhyay, M. Banerjee, Decarbonization of cooling of buildings, Sol. Compass. 2 (2022), 100025, https://doi.org/10.1016/J.SOLCOM.2022.100025.

[6] P.J. Gertler, O. Shelef, C.D. Wolfram, A. Fuchs, The demand for energy-using assets among the world's rising middle classes, Am. Econ. Rev. 106 (2016) 1366–1401, https://doi.org/10.1257/AER.20131455.

[7] R.E. López-Guerrero, K. Verichev, G.A. Moncada-Morales, M. Carpio, How do urban heat islands affect the thermo-energy performance of buildings? J. Clean. Prod. 373 (2022), 133713 https://doi.org/10.1016/J.JCLEPRO.2022.133713.

[8] Z. Ren, Y. Fu, Y. Dong, P. Zhang, X. He, Rapid urbanisation and climate change significantly contribute to worsening urban human thermal comfort: a national 183-city, 26-year study in China, Urban Clim. 43 (2022), 101154, https://doi.org/10.1016/J.UCLIM.2022.101154.

[9] IEA, The Future of Cooling, 2018, https://doi.org/10.1787/9789264301993-en.

[10] J. Bloomfield, F. Steward, The politics of the green new deal, Polit. Q. 91 (2020) 770–779, https://doi.org/10.1111/1467-923X.12917.

[11] G. Chiesa, M. Kolokotroni, P. Heiselberg, Springer, in: G. Chiesa, M. Kolokotroni, P. Heiselberg (Eds.), Innovations in Ventilative Cooling, Springer International Publishing, Cham, 2021, pp. 1–12, https://doi.org/10.1007/978-3-030-72385-9_1.

[12] V. IPCC, P. Masson-Delmotte, Zhai, A. Pirani, S.L. Connors, C. Péan, S. Berger, N. Caud, Y. Chen, L. Goldfarb, M.I. Gomis, M. Huang, K. Leitzell, E. Lonnoy, J.B. R. Matthews, T.K. Maycock, T. Waterfield, O. Yelekçi, R. Yu, Z. B, in: Climate Change 2021: the Physical Science Basis. Contribution of Working Group I to the Sixth Assessment Report of the Intergovernmental Panel on Climate Change, 2021. https://www.ipcc.ch/.

[13] J. Spinoni, J.V. Vogt, P. Barbosa, A. Dosio, N. McCormick, A. Bigano, H.M. Füssel, Changes of heating and cooling degree-days in Europe from 1981 to 2100, Int. J. Climatol. 38 (2018) e191–e208, https://doi.org/10.1002/JOC.5362.

[14] Y. Shi, D.F. Zhang, Y. Xu, B.T. Zhou, Changes of heating and cooling degree days over China in response to global warming of 1.5 °C, 2 °C, 3 °C and 4 °C, Adv. Clim. Change Res. 9 (2018) 192–200, https://doi.org/10.1016/J.ACCRE.2018.06.003.

[15] J. Xiong, S. Guo, Y. Wu, D. Yan, C. Xiao, X. Lu, Predicting the response of heating and cooling demands of residential buildings with various thermal performances in China to climate change, Energy 269 (2023), 126789, https://doi.org/10.1016/J.ENERGY.2023.126789.

[16] R. Ukey, A.C. Rai, Impact of global warming on heating and cooling degree days in major Indian cities, Energy Build. 244 (2021), 111050, https://doi.org/10.1016/J.ENBUILD.2021.111050.

[17] A.A. Alola, S. Saint Akadiri, A.C. Akadiri, U.V. Alola, A.S. Fatigun, Cooling and heating degree days in the US: the role of macroeconomic variables and its impact on environmental sustainability, Sci. Total Environ. 695 (2019), 133832, https://doi.org/10.1016/J.SCITOTENV.2019.133832.

[18] M.A.D. Larsen, S. Petrović, A.M. Radoszynski, R. McKenna, O. Balyk, Climate change impacts on trends and extremes in future heating and cooling demands over Europe, Energy Build. 226 (2020), 110397, https://doi.org/10.1016/j.enbuild.2020.110397.

[19] U. Berardi, P. Jafarpur, Assessing the impact of climate change on building heating and cooling energy demand in Canada, Renew. Sustain. Energy Rev. 121 (2020), 109681, https://doi.org/10.1016/j.rser.2019.109681.

[20] J.L. Fan, J.W. Hu, X. Zhang, Impacts of climate change on electricity demand in China: an empirical estimation based on panel data, Energy 170 (2019) 880–888, https://doi.org/10.1016/J.ENERGY.2018.12.044.

[21] P. Bezerra, F. da Silva, T. Cruz, M. Mistry, E. Vasquez-Arroyo, L. Magalar, E. De Cian, A.F.P. Lucena, R. Schaeffer, Impacts of a warmer world on space cooling demand in Brazilian households, Energy Build. 234 (2021), 110696, https://doi.org/10.1016/J.ENBUILD.2020.110696.

[22] J. Joshi, A. Magal, V.S. Limaye, P. Madan, A. Jaiswal, D. Mavalankar, K. Knowlton, Climate change and 2030 cooling demand in Ahmedabad, India: opportunities for expansion of renewable energy and cool roofs, Mitig. Adapt. Strategies Glob. Change 27 (2022) 44, https://doi.org/10.1007/S11027-022-10019-4.

[23] M. Sivak, Potential energy demand for cooling in the 50 largest metropolitan areas of the world: implications for developing countries, Energy Pol. 37 (2009) 1382–1384, https://doi.org/10.1016/J.ENPOL.2008.11.031.

[24] A.M. Khourchid, S.B. Ajjur, S.G. Al-Ghamdi, Building cooling requirements under climate change scenarios: impact, mitigation strategies, and future directions, 2022, Vol. 12, Page 1519, Build 12 (2022) 1519, https://doi.org/10.3390/BUILDINGS12101519.

[25] L. Bellani, M. Compare, E. Zio, A. Bosisio, B. Greco, G. Iannarelli, A. Morotti, A reliability-centred methodology for identifying renovation actions for improving resilience against heat waves in power distribution grids, Int. J. Electr. Power Energy Syst. 137 (2022), 107813, https://doi.org/10.1016/J.IJEPES.2021.107813.

[26] S. Attia, R. Levinson, E. Ndongo, P. Holzer, O. Berk Kazanci, S. Homaei, C. Zhang, B.W. Olesen, D. Qi, M. Hamdy, P. Heiselberg, Resilient cooling of buildings to protect against heat waves and power outages: key concepts and definition, Energy Build. 239 (2021), 110869.

[27] B. Stone, E. Mallen, M. Rajput, A. Broadbent, E.S. Krayenhoff, G. Augenbroe, M. Georgescu, Climate change and infrastructure risk: indoor heat exposure during a concurrent heat wave and blackout event in Phoenix, Arizona, Urban Clim. 36 (2021), 100787, https://doi.org/10.1016/J.UCLIM.2021.100787.

[28] U. Nations, D. of Economic, S. Affairs, P. Division, World Population Prospects 2022: Methodology of the United Nations Population Estimates and Projections, 2022. www.unpopulation.org.

[29] International Energy Agency, Studie, World Energy Outlook 2022, 2022. https://www.iea.org/reports/world-energy-outlook-2022.

[30] M. Santamouris, Cooling of buildings: the new energy challenge, Cool. Energy Solut. Build. Cities (2019) 1–16, https://doi.org/10.1142/9789813236974_0001.

[31] C. Mora, B. Dousset, I.R. Caldwell, F.E. Powell, R.C. Geronimo, C.R. Bielecki, C.W. W. Counsell, B.S. Dietrich, E.T. Johnston, L.V. Louis, M.P. Lucas, M.M. Mckenzie, A.G. Shea, H. Tseng, T.W. Giambelluca, L.R. Leon, E. Hawkins, C. Trauernicht, Global Risk of Deadly Heat, vol. 7, 2017, pp. 501–506. https://www.nature.com/articles/nclimate3322.

[32] S.L. de Moraes, R. Almendra, L.V. Barrozo, Impact of heat waves and cold spells on cause-specific mortality in the city of São Paulo, Brazil, Int. J. Hyg Environ. Health 239 (2022), 113861, https://doi.org/10.1016/J.IJHEH.2021.113861.

[33] A. Barreca, K. Clay, O. Deschenes, M. Greenstone, J.S. Shapiro, Adapting to climate change: the remarkable decline in the US temperature-mortality relationship over the Twentieth Century, J. Polit. Econ. 124 (2016) 105–159, https://doi.org/10.1086/684582.

[34] A. Nori-Sarma, G.B. Anderson, A. Rajiva, G. ShahAzhar, P. Gupta, M.S. Pednekar, J.Y. Son, R.D. Peng, M.L. Bell, The impact of heat waves on mortality in Northwest India, Environ. Res. 176 (2019), 108546, https://doi.org/10.1016/J.ENVRES.2019.108546.

[35] L. Davis, P. Gertler, S. Jarvis, C. Wolfram, Air conditioning and global inequality, Global Environ. Change 69 (2021), 102299, https://doi.org/10.1016/J.GLOENVCHA.2021.102299.

[36] O. Jay, A. Capon, P. Berry, C. Broderick, R. de Dear, G. Havenith, Y. Honda, R. S. Kovats, W. Ma, A. Malik, N.B. Morris, L. Nybo, S.I. Seneviratne, J. Vanos, K. L. Ebi, Reducing the health effects of hot weather and heat extremes: from personal cooling strategies to green cities, Lancet 398 (2021) 709–724, https://doi.org/10.1016/S0140-6736(21)01209-5.

[37] L. Borghero, E. Clèries, T. Péan, J. Ortiz, J. Salom, Comparing cooling strategies to assess thermal comfort resilience of residential buildings in Barcelona for present and future heatwaves, Build. Environ. 231 (2023), 110043, https://doi.org/10.1016/j.buildenv.2023.110043.

[38] R. Stasi, F. Ruggiero, U. Berardi, The efficiency of hybrid ventilation on cooling energy savings in NZEBs, J. Build. Eng. 53 (2022), 104401, https://doi.org/10.1016/j.jobe.2022.104401.

[39] IEA-EBC, IEA EBC Annex 80 - Resilient Cooling of Buildings, IEA EBC Annex 80 - Resilient Cool, 2023. Build, https://annex80.iea-ebc.org/.

[40] S. Flores-Larsen, C. Filippín, F. Bre, New metrics for thermal resilience of passive buildings during heat events, Build. Environ. 230 (2023), 109990, https://doi.org/10.1016/j.buildenv.2023.109990.

[41] K. Bamdad, S. Matour, N. Izadyar, S. Omrani, Impact of climate change on energy saving potentials of natural ventilation and ceiling fans in mixed-mode buildings, Build. Environ. 209 (2022), 108662, https://doi.org/10.1016/J.BUILDENV.2021.108662.

[42] International Energy Agency, Ventilative Cooling Design Guide- Energy in Buildings and Communities Programme, 2018. http://www.iea-ebc.org/Data/publications/EBC_Annex_62_Design_Guide.pdf.

[43] P. Heiselberg, Ventilative Cooling Principles, Potential and Barriers, Springer, 2021, pp. 15–37, https://doi.org/10.1007/978-3-030-72385-9_2.

[44] N. Artmann, H. Manz, P. Heiselberg, Climatic potential for passive cooling of buildings by night-time ventilation in Europe, Appl. Energy 84 (2007) 187–201, https://doi.org/10.1016/j.apenergy.2006.05.004.

[45] E. Tavakoli, A. O'Donovan, M. Kolokotroni, P.D. O'Sullivan, Evaluating the indoor thermal resilience of ventilative cooling in non-residential low energy buildings: a review, Build. Environ. 222 (2022), 109376, https://doi.org/10.1016/J.BUILDENV.2022.109376.

[46] E. López-García, J. Lizana, A. Serrano-Jiménez, C. Díaz-López, Ángela Barrios-Padura, Monitoring and analytics to measure heat resilience of buildings and support retrofitting by passive cooling, J. Build. Eng. 57 (2022), 104985, https://doi.org/10.1016/J.JOBE.2022.104985.

[47] N. Khan, Y. Su, S.B. Riffat, A review on wind driven ventilation techniques, Energy Build. 40 (2008) 1586–1604, https://doi.org/10.1016/J.ENBUILD.2008.02.015.

[48] B. Wang, A. Malkawi, Design-based natural ventilation evaluation in early stage for high performance buildings, Sustain. Cities Soc. 45 (2019) 25–37, https://doi.org/10.1016/j.scs.2018.11.024.

[49] T. Ahmed, P. Kumar, L. Mottet, Natural ventilation in warm climates: the challenges of thermal comfort, heatwave resilience and indoor air quality, Renew. Sustain. Energy Rev. 138 (2021), 110669, https://doi.org/10.1016/J.RSER.2020.110669.
[50] Y. Chen, Z. Tong, A. Malkawi, Investigating natural ventilation potentials across the globe: regional and climatic variations, Build. Environ. 122 (2017) 386–396, https://doi.org/10.1016/j.buildenv.2017.06.026.
[51] D.K. Bhamare, M.K. Rathod, J. Banerjee, Passive cooling techniques for building and their applicability in different climatic zones—the state of art, Energy Build. 198 (2019) 467–490, https://doi.org/10.1016/J.ENBUILD.2019.06.023.
[52] M. Lee, D. Cha, S. Yun, S.M. Yoon, Y. Kim, Comparative heating performance evaluation of hybrid ground-source heat pumps using serial and parallel configurations with the application of ground heat exchanger, Energy Convers. Manag. 229 (2021), 113743, https://doi.org/10.1016/j.enconman.2020.113743.
[53] H. Cho, D. Cabrera, S. Sardy, R. Kilchherr, S. Yilmaz, M.K. Patel, Evaluation of performance of energy efficient hybrid ventilation system and analysis of occupants' behavior to control windows, Build. Environ. 188 (2021), 107434, https://doi.org/10.1016/j.buildenv.2020.107434.
[54] G. Chiesa, EAHX – earth-to-air heat exchanger: simplified method and KPI for early building design phases, Build. Environ. 144 (2018) 142–158, https://doi.org/10.1016/j.buildenv.2018.08.014.
[55] R. Stasi, S. Liuzzi, S. Paterno, F. Ruggiero, P. Stefanizzi, A. Stragapede, Combining bioclimatic strategies with efficient HVAC plants to reach nearly-zero energy building goals in Mediterranean climate, Sustain. Cities Soc. 63 (2020), https://doi.org/10.1016/j.scs.2020.102479.
[56] J. Guo, J. Dong, B. Zou, H. Wang, L. Zhu, Y. Jiang, Experimental investigation on the effects of phase change material and different ventilation modes on the thermal storage, space heating and energy consumption characteristics of ventilated mortar blocks, J. Energy Storage 41 (2021), 102817, https://doi.org/10.1016/J.EST.2021.102817.
[57] X. Jia, J. Wang, Y. Zhu, W. Ji, B. Cao, Cooling effect of elevated ambient air velocity on thermal comfort when sitting after walking, Build. Environ. 225 (2022), 109664, https://doi.org/10.1016/j.buildenv.2022.109664.
[58] D. Wang, C. Song, Y. Wang, Y. Xu, Y. Liu, J. Liu, Experimental investigation of the potential influence of indoor air velocity on students' learning performance in summer conditions, Energy Build. 219 (2020), 110015, https://doi.org/10.1016/J.ENBUILD.2020.110015.
[59] N. Kumar, T. Kubota, Y. Tominaga, M. Shirzadi, R. Bardhan, CFD simulations of wind-induced ventilation in apartment buildings with vertical voids: effects of pilotis and wind fin on ventilation performance, Build. Environ. 194 (2021), 107666, https://doi.org/10.1016/J.BUILDENV.2021.107666.
[60] R. de Dear, J. Xiong, J. Kim, B. Cao, A review of adaptive thermal comfort research since 1998, Energy Build. 214 (2020), 109893.
[61] R. Stasi, F. Ruggiero, U. Berardi, Evaluation of mixed mode ventilation cooling energy saving potential in nZEB: a case study in Southern Italy, E3S Web Conf. 343 (2022), 01004, https://doi.org/10.1051/E3SCONF/202234301004.
[62] Y. Peng, Y. Lei, Z.D. Tekler, N. Antanuri, S.K. Lau, A. Chong, Hybrid system controls of natural ventilation and HVAC in mixed-mode buildings: a comprehensive review, Energy Build. 276 (2022), 112509, https://doi.org/10.1016/J.ENBUILD.2022.112509.
[63] N.R.M. Sakiyama, L. Mazzaferro, J.C. Carlo, T. Bejat, H. Garrecht, Natural ventilation potential from weather analyses and building simulation, Energy Build. 231 (2021), 110596, https://doi.org/10.1016/J.ENBUILD.2020.110596.
[64] E. Mushtaha, T. Salameh, S. Kharrufa, T. Mori, A. Aldawoud, R. Hamad, T. Nemer, The impact of passive design strategies on cooling loads of buildings in temperate climate, Case Stud. Therm. Eng. 28 (2021), 101588, https://doi.org/10.1016/J.CSITE.2021.101588.
[65] S. Erba, A. Sangalli, L. Pagliano, Present and future potential of natural night ventilation in nZEBs, IOP Conf. Ser. Earth Environ. Sci. 296 (2019), 012041, https://doi.org/10.1088/1755-1315/296/1/012041.
[66] H. Campaniço, P.M.M. Soares, R.M. Cardoso, P. Hollmuller, Impact of climate change on building cooling potential of direct ventilation and evaporative cooling: a high resolution view for the Iberian Peninsula, Energy Build. 192 (2019) 31–44, https://doi.org/10.1016/J.ENBUILD.2019.03.017.
[67] C. Li, Y. Chen, A multi-factor optimization method based on thermal comfort for building energy performance with natural ventilation, Energy Build. 285 (2023), 112893, https://doi.org/10.1016/J.ENBUILD.2023.112893.
[68] Y. Chen, Z. Tong, W. Wu, H. Samuelson, A. Malkawi, L. Norford, Achieving natural ventilation potential in practice: control schemes and levels of automation, Appl. Energy 235 (2019) 1141–1152, https://doi.org/10.1016/J.APENERGY.2018.11.016.
[69] J.W. Axley, Application of Natural Ventilation for U.S. Commerical Buildings : Climate Suitability Design Strategies and Methods Modeling Studies, 2001, https://doi.org/10.6028/NIST.GCR.01-820.
[70] W. Yin, G. Zhang, W. Yang, X. Wang, Natural ventilation potential model considering solution multiplicity, window opening percentage, air velocity and humidity in China, Build. Environ. 45 (2010) 338–344, https://doi.org/10.1016/j.buildenv.2009.06.012.
[71] S. Schiavon, A.K. Melikov, Energy saving and improved comfort by increased air movement, Energy Build. 40 (2008) 1954–1960, https://doi.org/10.1016/J.ENBUILD.2008.05.001.
[72] C. Hirose, N. Ikegaya, A. Hagishima, J. Tanimoto, Indoor airflow and thermal comfort in a cross-ventilated building within an urban-like block array using large-eddy simulations, Build. Environ. 196 (2021), 107811, https://doi.org/10.1016/J.BUILDENV.2021.107811.
[73] Z. Jiang, T. Kobayashi, T. Yamanaka, M. Sandberg, A literature review of cross ventilation in buildings, Energy Build. 291 (2023), 113143, https://doi.org/10.1016/j.enbuild.2023.113143.
[74] S. Omrani, V. Garcia-Hansen, B.R. Capra, R. Drogemuller, Effect of natural ventilation mode on thermal comfort and ventilation performance: full-scale measurement, Energy Build. 156 (2017) 1–16, https://doi.org/10.1016/j.enbuild.2017.09.061.
[75] E. Spentzou, M.J. Cook, S. Emmitt, Natural ventilation strategies for indoor thermal comfort in Mediterranean apartments, Build. Simulat. 11 (2018) 175–191, https://doi.org/10.1007/S12273-017-0380-1/METRICS.
[76] N. Nasrollahi, P. Ghobadi, Field measurement and numerical investigation of natural cross-ventilation in high-rise buildings; Thermal comfort analysis, Appl. Therm. Eng. 211 (2022), 118500, https://doi.org/10.1016/J.APPLTHERMALENG.2022.118500.
[77] U. Passe, F. Battaglia, Designing Spaces for Natural Ventilation: an Architect's Guide, Routledge, 2015. https://books.google.it/books?id=GMIqBwAAQBAJ&printsec=copyright&redir_esc=y#v=onepage&q&f=false.
[78] K.B. Fernandez, N. Ikegaya, K. Ito, Q. Chen, Age of air, purging flow rate, and net escape velocity in a cross-ventilation model sheltered by urban-like blocks using LES, Build. Environ. 226 (2022), 109759, https://doi.org/10.1016/J.BUILDENV.2022.109759.
[79] T.E. Morakinyo, W. Ouyang, K.K.L. Lau, C. Ren, E. Ng, Right tree, right place (urban canyon): tree species selection approach for optimum urban heat mitigation - development and evaluation, Sci. Total Environ. (2020), https://doi.org/10.1016/j.scitotenv.2020.137461.
[80] E. Bay, A. Martinez-Molina, W.A. Dupont, Assessment of natural ventilation strategies in historical buildings in a hot and humid climate using energy and CFD simulations, J. Build. Eng. 51 (2022), 104287, https://doi.org/10.1016/J.JOBE.2022.104287.
[81] H. Hu, H. Kikumoto, R. Ooka, C. Lin, B. Zhang, Comprehensive validation of experimental and numerical natural ventilation predictions based on field measurement with experimental house, Build. Environ. 207 (2022), 108433, https://doi.org/10.1016/J.BUILDENV.2021.108433.
[82] K. Kosutova, T. van Hooff, C. Vanderwel, B. Blocken, J. Hensen, Cross-ventilation in a generic isolated building equipped with louvers: wind-tunnel experiments and CFD simulations, Build. Environ. 154 (2019) 263–280, https://doi.org/10.1016/J.BUILDENV.2019.03.019.
[83] M. Shirzadi, Y. Tominaga, P.A. Mirzaei, Experimental Study on Cross-Ventilation of a Generic Building in Highly-Dense Urban Areas: Impact of Planar Area Density and Wind Direction, 2019, https://doi.org/10.1016/j.jweia.2019.104030.
[84] Q. Yi, G. Zhang, M. König, D. Janke, S. Hempel, T. Amon, Investigation of discharge coefficient for wind-driven naturally ventilated dairy barns, Energy Build. 165 (2018) 132–140, https://doi.org/10.1016/j.enbuild.2018.01.038.
[85] B. Blocken, 50 years of computational wind engineering: past, present and future, J. Wind Eng. Ind. Aerod. 129 (2014) 69–102, https://doi.org/10.1016/J.JWEIA.2014.03.008.
[86] X. Zhang, A.U. Weerasuriya, J. Wang, C.Y. Li, Z. Chen, K.T. Tse, J. Hang, Cross-ventilation of a generic building with various configurations of external and internal openings, Build. Environ. 207 (2022), 108447, https://doi.org/10.1016/j.buildenv.2021.108447.
[87] K.S. Jon, Y. Luo, C.H. Sin, P. yi Cui, Y. dong Huang, J. Tokgo, Impacts of wind direction on the ventilation and pollutant dispersion of 3D street canyon with balconies, Build. Environ. 230 (2023), 110034, https://doi.org/10.1016/J.BUILDENV.2023.110034.
[88] M. Shirzadi, P.A. Mirzaei, M. Naghashzadegan, Y. Tominaga, Modelling enhancement of cross-ventilation in sheltered buildings using stochastic optimization, Int. J. Heat Mass Tran. 118 (2018) 758–772, https://doi.org/10.1016/J.IJHEATMASSTRANSFER.2017.10.107.
[89] M. Shirzadi, P.A. Mirzaei, Y. Tominaga, CFD analysis of cross-ventilation flow in a group of generic buildings: comparison between steady RANS, LES and wind tunnel experiments, Build. Simulat. 13 (2020) 1353–1372, https://doi.org/10.1007/S12273-020-0657-7/METRICS.
[90] A. Ricci, I. Kalkman, B. Blocken, M. Burlando, M.P. Repetto, Impact of turbulence models and roughness height in 3D steady RANS simulations of wind flow in an urban environment, Build. Environ. 171 (2020), 106617, https://doi.org/10.1016/J.BUILDENV.2019.106617.
[91] F. Jiang, S. Tao, Q. Tao, zhengrong Li, Y. Yuan, J. Zheng, The effect of louver blinds on the wind-driven cross ventilation of multi-storey buildings, J. Build. Eng. 54 (2022), 104614, https://doi.org/10.1016/J.JOBE.2022.104614.
[92] W. Zhong, W. Xiao, T. Zhang, Numerical investigations on natural ventilation in atria of China's southern yangtze vernacular dwellings, Sustain. Cities Soc. 89 (2023), 104341, https://doi.org/10.1016/J.SCS.2022.104341.
[93] Z. Zhiyi, Y. Wei, W. Tianwen, L. Yonghan, Z. Yawen, Z. Guoqiang, Potential of cross-ventilation channels in an ideal typical apartment building predicted by CFD and multi-zone airflow model, J. Build. Eng. 44 (2021), 103408, https://doi.org/10.1016/j.jobe.2021.103408.
[94] S. Agrawal, J.K. Wong, J. Song, O. Mercan, P.J. Kushner, Assessment of the aerodynamic performance of unconventional building shapes using 3D steady RANS with SST k-ω turbulence model, J. Wind Eng. Ind. Aerod. 225 (2022), 104988, https://doi.org/10.1016/J.JWEIA.2022.104988.
[95] H. Montazeri, B. Blocken, CFD simulation of wind-induced pressure coefficients on buildings with and without balconies: validation and sensitivity analysis, Build. Environ. 60 (2013) 137–149, https://doi.org/10.1016/J.BUILDENV.2012.11.012.
[96] S.F. Díaz-Calderón, J.A. Castillo, G. Huelsz, Evaluation of different window heights and facade porosities in naturally cross-ventilated buildings: CFD

validation, J. Wind Eng. Ind. Aerod. 232 (2023), 105263, https://doi.org/10.1016/J.JWEIA.2022.105263.
[97] P.D. O'Sullivan, M. Kolokotroni, A field study of wind dominant single sided ventilation through a narrow slotted architectural louvre system, Energy Build. 138 (2017) 733–747, https://doi.org/10.1016/J.ENBUILD.2016.11.025.
[98] Y. Tominaga, B. Blocken, Wind tunnel analysis of flow and dispersion in cross-ventilated isolated buildings: impact of opening positions, J. Wind Eng. Ind. Aerod. 155 (2016) 74–88, https://doi.org/10.1016/J.JWEIA.2016.05.007.
[99] J.I. Perén, T. van Hooff, B.C.C. Leite, B. Blocken, CFD analysis of cross-ventilation of a generic isolated building with asymmetric opening positions: impact of roof angle and opening location, Build. Environ. 85 (2015) 263–276, https://doi.org/10.1016/j.buildenv.2014.12.007.
[100] F. Bazdidi-Tehrani, S. Masoumi-Verki, P. Gholamalipour, Impact of opening shape on airflow and pollutant dispersion in a wind-driven cross-ventilated model building: large eddy simulation, Sustain. Cities Soc. 61 (2020), 102196, https://doi.org/10.1016/J.SCS.2020.102196.
[101] W. Zhong, T. Zhang, T. Tamura, CFD simulation of convective heat transfer on vernacular sustainable architecture: validation and application of methodology, Sustain. Times 11 (2019), https://doi.org/10.3390/su11154231.
[102] T. van Hooff, B. Blocken, Y. Tominaga, On the accuracy of CFD simulations of cross-ventilation flows for a generic isolated building: comparison of RANS, LES and experiments, Build. Environ. 114 (2017) 148–165, https://doi.org/10.1016/J.BUILDENV.2016.12.019.
[103] X. Zhang, A.U. Weerasuriya, K.T. Tse, CFD simulation of natural ventilation of a generic building in various incident wind directions: comparison of turbulence modelling, evaluation methods, and ventilation mechanisms, Energy Build. 229 (2020), 110516, https://doi.org/10.1016/J.ENBUILD.2020.110516.
[104] P.H.V. Nimarshana, R.A. Attalage, K.K.C.K. Perera, Quantification of the impact of RANS turbulence models on airflow distribution in horizontal planes of a generic building under cross-ventilation for prediction of indoor thermal comfort, J. Build. Eng. 52 (2022), 104409, https://doi.org/10.1016/J.JOBE.2022.104409.
[105] J.I. Perén, T. van Hooff, B.C.C. Leite, B. Blocken, CFD simulation of wind-driven upward cross ventilation and its enhancement in long buildings: impact of single-span versus double-span leeward sawtooth roof and opening ratio, Build. Environ. 96 (2016) 142–156, https://doi.org/10.1016/J.BUILDENV.2015.11.021.
[106] R. Ramponi, B. Blocken, CFD simulation of cross-ventilation for a generic isolated building: impact of computational parameters, Build. Environ. 53 (2012) 34–48, https://doi.org/10.1016/J.BUILDENV.2012.01.004.
[107] D. Mohotti, K. Wijesooriya, D. Dias-da-Costa, Comparison of Reynolds Averaging Navier-Stokes (RANS) turbulent models in predicting wind pressure on tall buildings, J. Build. Eng. 21 (2019) 1–17, https://doi.org/10.1016/J.JOBE.2018.09.021.
[108] M. Rodríguez-Vázquez, I. Hernández-Pérez, J. Xamán, Y. Chávez, M. Gijón-Rivera, J.M. Belman-Flores, Coupling building energy simulation and computational fluid dynamics: an overview, J. Build. Phys. 44 (2020) 137–180, https://doi.org/10.1177/1744259120901840.
[109] F. Xu, S. Xu, U. Passe, B. Ganapathysubramanian, Computational study of natural ventilation in a sustainable building with complex geometry, Sustain. Energy Technol. Assessments 45 (2021), 101153, https://doi.org/10.1016/j.seta.2021.101153.
[110] Y. Vaishnani, S.F. Ali, A. Joshi, D. Rakshit, F. Wang, Thermal performance analysis of a naturally ventilated system using PMV models for different roof inclinations in composite climatic conditions, J. Brazilian Soc. Mech. Sci. Eng. 42 (2020) 1–16, https://doi.org/10.1007/S40430-020-2219-4/FIGURES/12.
[111] Y. Tominaga, A. Mochida, R. Yoshie, H. Kataoka, T. Nozu, M. Yoshikawa, T. Shirasawa, AIJ guidelines for practical applications of CFD to pedestrian wind environment around buildings, J. Wind Eng. Ind. Aerod. 96 (2008) 1749–1761, https://doi.org/10.1016/J.JWEIA.2008.02.058.
[112] P. Heiselberg, Modelling of Natural and Hybrid Ventilation, Aalborg Univ., 2006, p. 54.
[113] C. Ghiaus, F. Allard, The physics of natural ventilation, in: Nat. Vent. Urban Environ. Assess. Des., Routledge, 2012, pp. 36–80, https://doi.org/10.4324/9781849772068.
[114] Ashrae, ANSI/ASHRAE Standard 55-2020, 2021. www.ashrae.org.
[115] S. Carlucci, L. Bai, R. de Dear, L. Yang, Review of adaptive thermal comfort models in built environmental regulatory documents, Build. Environ. 137 (2018) 73–89, https://doi.org/10.1016/J.BUILDENV.2018.03.053.
[116] R. Yao, S. Zhang, C. Du, M. Schweiker, S. Hodder, B.W. Olesen, J. Toftum, F. Romana d'Ambrosio, H. Gebhardt, S. Zhou, F. Yuan, B. Li, Evolution and performance analysis of adaptive thermal comfort models – a comprehensive literature review, Build. Environ. 217 (2022), 109020, https://doi.org/10.1016/J.BUILDENV.2022.109020.
[117] S. Manu, Y. Shukla, R. Rawal, L.E. Thomas, R. de Dear, Field studies of thermal comfort across multiple climate zones for the subcontinent: India Model for Adaptive Comfort (IMAC), Build, Environ. Times 98 (2016) 55–70, https://doi.org/10.1016/J.BUILDENV.2015.12.019.
[118] D.K. Bhamare, M.K. Rathod, J. Banerjee, Evaluation of cooling potential of passive strategies using bioclimatic approach for different Indian climatic zones, J. Build. Eng. 31 (2020), 101356, https://doi.org/10.1016/J.JOBE.2020.101356.
[119] R. Rawal, Y. Shukla, V. Vardhan, S. Asrani, M. Schweiker, R. de Dear, V. Garg, J. Mathur, S. Prakash, S. Diddi, S.V. Ranjan, A.N. Siddiqui, G. Somani, Adaptive thermal comfort model based on field studies in five climate zones across India, Build. Environ. 219 (2022), 109187, https://doi.org/10.1016/J.BUILDENV.2022.109187.
[120] S. Carlucci, S. Erba, L. Pagliano, R. de Dear, ASHRAE Likelihood of Dissatisfaction: a new right-here and right-now thermal comfort index for assessing the Likelihood of dissatisfaction according to the ASHRAE adaptive comfort model, Energy Build. 250 (2021), 111286, https://doi.org/10.1016/J.ENBUILD.2021.111286.
[121] S. Carlucci, A review of long-term discomfort indices, SpringerBriefs Appl. Sci. Technol. (2013) 1–20, https://doi.org/10.1007/978-88-470-5238-3_1.
[122] S. Carlucci, L. Pagliano, A. Sangalli, Statistical analysis of the ranking capability of long-term thermal discomfort indices and their adoption in optimization processes to support building design, Build. Environ. 75 (2014) 114–131, https://doi.org/10.1016/J.BUILDENV.2013.12.017.
[123] A. Dhalluin, K. Limam, in: Comparison of Natural and Hybrid Ventilation Strategies Used in Classrooms in Terms of Indoor Environmental Quality, Comfort and Energy Savings, vol. 23, 2012, pp. 527–542, https://doi.org/10.1177/1420326X12464077.
[124] V. Cheng, E. Ng, in: Comfort Temperatures for Naturally Ventilated Buildings in Hong Kong, vol. 49, 2011, pp. 179–182, https://doi.org/10.3763/ASRE.2006.4924.
[125] D. Gupta, V.R. Khare, Natural ventilation design: predicted and measured performance of a hostel building in composite climate of India, Energy Built Environ. 2 (2021) 82–93.
[126] M. Doctor-Pingel, V. Vardhan, S. Manu, G. Brager, R. Rawal, A study of indoor thermal parameters for naturally ventilated occupied buildings in the warm-humid climate of southern India, Build. Environ. 151 (2019) 1–14, https://doi.org/10.1016/j.buildenv.2019.01.026.
[127] Z. Tong, Y. Chen, A. Malkawi, Defining the Influence Region in neighborhood-scale CFD simulations for natural ventilation design, Appl. Energy 182 (2016) 625–633, https://doi.org/10.1016/J.APENERGY.2016.08.098.
[128] M. Shirzadi, Y. Tominaga, P.A. Mirzaei, Wind tunnel experiments on cross-ventilation flow of a generic sheltered building in urban areas, Build. Environ. 158 (2019) 60–72, https://doi.org/10.1016/J.BUILDENV.2019.04.057.
[129] A. Ricci, M. Guasco, F. Caboni, M. Orlanno, A. Giachetta, M.P. Repetto, Impact of surrounding environments and vegetation on wind comfort assessment of a new tower with vertical green park, Build. Environ. 207 (2022), 108409, https://doi.org/10.1016/J.BUILDENV.2021.108409.
[130] Z. Tong, Y. Chen, A. Malkawi, Estimating natural ventilation potential for high-rise buildings considering boundary layer meteorology, Appl. Energy 193 (2017) 276–286, https://doi.org/10.1016/J.APENERGY.2017.02.041.
[131] J. Hang, Z. Luo, M. Sandberg, J. Gong, Natural ventilation assessment in typical open and semi-open urban environments under various wind directions, Build. Environ. 70 (2013) 318–333, https://doi.org/10.1016/J.BUILDENV.2013.09.002.